Two coupled feedback loops explain random mono-allelic *Xist* upregulation at the onset of X-chromosome inactivation

Verena Mutzel[1], Ikuhiro Okamoto[2], Ilona Dunkel[1], Mitinori Saitou[3], Luca Giorgetti[4], Edith Heard[5], Edda G. Schulz*[1]

Summary

In female mammals, dosage compensation for X-linked genes is ensured through random X-chromosome inactivation, which is initiated by mono-allelic up-regulation of *Xist*. We use mathematical modeling to identify the regulatory principles required to establish the mono-allelic and female-specific *Xist* expression pattern and test model predictions experimentally. A *cis*-acting positive feedback, which in mice is mediated by mutual repression of *Xist* and its antisense transcript *Tsix*, together with a *trans*-acting negative feedback are sufficient to explain mono-allelic *Xist* up-regulation. The model can reproduce data from several mutant, aneuploid and polyploid murine cell lines and explains *Xist* expression patterns in other mammalian species. Furthermore, it predicts that transient, reversible bi-allelic *Xist* expression is not restricted to rabbits and humans but can also occur in mice, which we indeed confirm to occur in mouse embryos. Overall, our study provides a conceptual framework of the molecular mechanisms required to initiate random X-chromosome inactivation.

Keywords: X-chromosome inactivation, gene-regulatory networks, mathematical modelling, feedback loops, systems biology, mono-allelic expression, transcriptional interference, antisense transcription,

[1] Regulatory Networks in Stem Cells, Otto-Warburg-Laboratorium, Max Planck Institute for molecular Genetics, 14195 Berlin, Germany

[2] Department of Anatomy and Cell Biology, Graduate School of Medicine, Kyoto University, 606-8501, Japan; JST, ERATO, Kyoto 606-8501, Japan

[3] Department of Anatomy and Cell Biology, Graduate School of Medicine, Kyoto University, 606-8501, Japan; JST, ERATO, Kyoto 606-8501, Japan; Center for iPS Cell Research and Application, Kyoto University, Kyoto 606-8507, Japan; Institute for Integrated Cell-Material Sciences, Kyoto University, Kyoto 606-8501, Japan.

[4] Friedrich Miescher Institute for Biomedical Research, Basel, CH-4058, Switzerland

[5] Institut Curie, PSL Research University, CNRS UMR3215, INSERM U934, Paris, France

* Corresponding Author: edda.schulz@molgen.mpg.de

Introduction

To achieve dosage compensation between the sexes, eutherian mammals have evolved the process of X-chromosome inactivation (XCI) where one randomly chosen X-chromosome in each female cell is silenced. XCI is initiated during early embryonic development through up-regulation of the long noncoding RNA *Xist* from one X-chromosome, which then mediates chromosome-wide gene silencing *in cis* (Augui et al., 2011). *Xist* recruits several repressive histone modifications including H3K27me3 to the inactive X, eventually resulting in complete heterochromatinization of the entire chromosome. While *Xist* appears to control XCI in all eutherian mammals, marked differences have been found in the way it is regulated (Sado and Sakaguchi, 2013). While human and rabbit embryos pass through an initial stage where *Xist* is expressed from both X chromosomes, no bi-allelic *Xist* up-regulation has been observed in mouse embryos (Mak et al., 2004; Okamoto et al., 2004; 2011). Although all these species exhibit random XCI in somatic tissues, they have been suggested to employ different strategies for its initial establishment during embryogenesis.

To establish the female-specific mono-allelic expression pattern of *Xist*, the cell must assess the number X-chromosomes that are present, choose one of them for *Xist* up-regulation and stabilize the two opposing states of the inactive X (Xi), which expresses *Xist*, and the active X (Xa) where *Xist* is silent (Augui et al., 2011). To explain how a cell assesses whether more than one X chromosome is present, a so-called X-linked competence factor or X-linked *Xist* Activator (XXA) has been predicted based on the different XCI patterns observed in cells with mutant or supernumerary X chromosomes: *Xist* is up-regulated in female cells with two or more X chromosomes, but not in male or XO cells with only a single X (Brown et al., 1992). Since the XXA would be encoded on the X chromosome, it would be present in a double dose in female compared to male cells. Assuming that XXA must exceed a certain threshold to up-regulate *Xist* in a dose-dependent manner, it could ensure female-specificity of XCI. Interestingly, diploid cells with four X chromosomes (X tetrasomy) inactivate three X's (Brown et al., 1992), while tetraploid cells that also contain four X chromosomes only inactivate two of them (Monkhorst et al., 2008), suggesting that autosomal ploidy also modulates the onset of XCI.

The "choice" process presumably involves a symmetry-breaking event between the two homologous X chromosomes, potentially mediated by fluctuation of *Xist* expression, or its regulators. Such fluctuations might be associated with homologous pairing (Bacher et al. 2006; Nicodemi and Prisco, 2007; Xu, 2006), or with alternative 3D conformations of

the *Xist* locus (Giorgetti et al., 2014). A "stochastic model of XCI" has been proposed whereby initially each chromosome can up-regulate *Xist* independently in a stochastic manner (Monkhorst et al., 2008; 2009). Through silencing of the XXA upon initiation of XCI, the XXA dose will drop below the predicted threshold and only a single dose of the activator as present in male cells will remain, which is not sufficient to up-regulate *Xist* from the second chromosome. In this model, XXA silencing would constitute a negative feedback to prevent bi-allelic *Xist* up-regulation. It however remains to be addressed how such a sharp threshold can be established that can distinguish between a single and a double dose of XXA and how maintenance of the asymmetric Xa/Xi state is ensured, which requires rapid stabilization of the *Xist*-expressing and the *Xist*-silent states in the presence of a single XXA dose.

A series of molecular regulators have been identified to be involved in the establishment of female-specific mono-allelic *Xist* expression. To control the developmental timing of *Xist* expression, several pluripotency factors repress *Xist* and their down-regulation during differentiation has been suggested to be required for *Xist* up-regulation (Navarro and Avner, 2010). Moreover, (transient) down-regulation of *Tsix*, a *cis*-acting repressor of *Xist* might trigger *Xist* up-regulation and thereby contribute to the "choice" process (Lee and Lu, 1999). *Tsix* is transcribed through *Xist* and its promoter in the antisense direction and induces a repressed chromatin state at the *Xist* promoter (Navarro et al., 2006; Sado et al., 2005). Two other X-linked genes, *Rnf12/Rlim* and *Jpx*, have been suggested to mediate sensing of the presence of more than one X by activating *Xist* in *trans*. However, neither of them exhibits the full phenotype expected from the XXA. While *Rnf12* can induce *Xist* up-regulation when overexpressed in male cells, its heterozygous deletion resulting in a single dose as in male cells does not prevent XCI (Jonkers et al., 2009). The ability of *Jpx* to up-regulate *Xist in trans* is controversial, since one study found that a heterozygous deletion of *Jpx* prevented XCI (Di Tian et al., 2010), while another report could not detect such a phenotype (Barakat et al., 2014) and an extra copy of *Jpx* is insufficient to up-regulate *Xist* (Heard et al., 1999).

Although a series of hypotheses about how female-specific and mono-allelic *Xist* up-regulation is ensured have been developed over the years and several regulators of *Xist* have been identified, the underlying regulatory principles and their molecular implementation remain largely unknown. We therefore present an alternative approach, where the regulatory interactions required to establish and maintain mono-allelic *Xist* expression are identified by mathematical modeling and are then tested experimentally. We show that stochastic *Xist* up-regulation and a *trans*-acting negative feedback loop must be combined with a *cis*-acting positive feedback to maintain mono-allelic *Xist* expression. Proposing that the predicted positive feedback loop is mediated by mutual repression of *Xist* and *Tsix*, we develop a detailed model, which reproduces several

3

observations previously made in *Xist* and *Tsix* mutant mouse embryonic stem cell lines. Moreover, the model predicts some level of transient bi-allelic expression, which we confirm to occur in mouse embryos *in vivo* and which we show to be reversible through experiments in embryonic stem cells. We thus present a comprehensive model of the gene-regulatory network that governs initiation and maintenance of mono-allelic *Xist* expression.

Results

Maintenance of mono-allelic *Xist* expression requires a *cis*-acting positive feedback loop

The inactive X (Xi), where *Xist* is transcribed, and the active X (Xa), where *Xist* is silent maintain two opposing expression states of *Xist* within the same nucleus. We first asked which regulatory interactions are required to stably maintain the correct *Xist* expression pattern. To this end, we compared a series of network architectures through mathematical modeling and simulations with respect to their ability to (1) maintain mono-allelic *Xist* expression, (2) to prevent bi-allelic *Xist* up-regulation and (3) to prevent *Xist* expression in male cells.

The models describe the population-averaged behavior of a cell with two X chromosomes harboring *Xist* and a trans-acting *XXA* gene, which activates *Xist* expression (Fig. 1A). We first tested a model where XXA escapes XCI (Model A), which is the case for the XXA candidate *Jpx* (Di Tian et al., 2010), and a network where XXA is silenced by *Xist in cis* and thus forms a negative feedback loop (Model B), which is the case for *Rnf12* (Jonkers et al., 2009). Each network was described in terms of ordinary differential equations (ODE) describing transcription and degradation dynamics of *Xist* and XXA and how they interact through mutual regulation of their transcription rates (see supplemental methods). Since the rates, ie. the model parameters, are unknown, we tested 1000 randomly chosen parameter sets, where transcription rates were varied between 10 and 1000 molecules/h and different degrees of non-linearity were tested (see supplemental procedures). To understand whether mono-allelic expression can be maintained by either of these two simple networks, both models were simulated starting from a mono-allelic state where one chromosome expresses high levels of *Xist* (Xi), while *Xist* is silent on the other allele (Xa) (Fig. 1B, Model A+B). When analyzing the state reached after 10,000 h of simulation we found that the mono-allelic state of *Xist* could not be maintained by either network (Fig. 1B+E, Model A+B).

4

These simulations show that the simple networks tested are not able to maintain two alternative expression states for the Xa and Xi. In other biological contexts (e.g. in the context of cell fate decisions), positive feedback loops, which can lead to bistability, have been found to generate alternative states. We therefore hypothesized that a positive feedback loop controlling *Xist* expression *in cis* could allow the two alleles to maintain distinct states and thus keep a memory of the initial decision of which allele would be the Xi and Xa, respectively. Such a positive feedback loop was added to each of the two previously proposed models (resulting in Models C and D, Fig. 1A) and again the steady states reached from mono-allelic initial conditions were simulated. In both cases a subset of the tested parameter sets were able to maintain mono-allelic expression (Fig. 1B+E, Model C+D), showing that a positive feedback loop can indeed stabilize two opposing transcriptional states on the two alleles. When analyzing the mono-allelic parameter sets, we found that some degree of non-linearity (Hill coefficient>=2) was required in the positive feedback loop (see supplemental material). Such non-linear interactions create an activation threshold, and once the *Xist* level exceeds this threshold the system can transition to the high *Xist* expression state (Xi).

In the next step, we addressed the role of the negative feedback loop, which has been suggested to play an important role in preventing bi-allelic *Xist* up-regulation. We re-simulated all mono-allelic parameter sets (i.e. those that were able to maintain the mono-allelic state in Simulation 1), but starting from a bi-allelic expression state (XiXi) where both alleles express *Xist* (Figure 1C). This analysis revealed that only for the model containing a negative feedback loop (Model D) parameter sets could be found where bi-allelic expression was unstable (Fig. 1C+E Simulation 2). Finally, we tested whether the same model would also be able to prevent *Xist* expression in male cells. Starting from an *Xist*-expressing initial state, we simulated a male cell containing only one copy of *Xist* and *XXA* and thus produces half the level of XXA compared to a female cell (Figure 1D). For all parameter sets where the XaXi state was stable in Simulation 1, while the XiXi state was unstable in Simulation 2, we found that *Xist* expression was not maintained at the single X in male cells (Fig. 1D+E, Simulation 3). Through comparison of four different network architectures and systematic parameter scanning, we could thus show that a *cis*-acting positive feedback loop and a *trans*-acting negative feedback can together maintain *Xist* mono-allelic expression, prevent bi-allelic up-regulation and prevent sustained *Xist* expression in male cells.

Mutual repression of *Xist* and *Tsix* can maintain the mono-allelic state

Our model comparison predicts that a *cis*-acting positive feedback loop is necessary to stabilize *Xist* expression from the inactive X-chromosome. We hypothesized that such a feedback loop could be mediated by mutual repression of *Xist* and its antisense

transcript *Tsix*. *Tsix* is a well-known *cis*-acting repressor of *Xist*, which can in turn be silenced *in cis* by *Xist* RNA like other X-linked genes. However, the exact molecular details by which *Tsix* exerts its repressive function on *Xist* are unknown. To address this question, we developed a detailed mathematical model of the *Xist/Tsix* locus describing transcriptional initiation, RNA PolII elongation and RNA degradation of this antisense gene pair (Fig. 2A). We hypothesized that mutual *Xist/Tsix* repression occurs by at least three distinct mechanisms: (1) *Xist* RNA-dependent silencing of the *Tsix* promoter, (2) *Tsix*-dependent repression of the *Xist* promoter and (3) transcriptional interference through collisions of RNA Pol II. While degradation and elongation rates were set to fixed values that have previously been estimated experimentally (detail given in supplemental material), transcription initiation rates of *Xist* and *Tsix* are unknown and values between 10 and 1000 molecules/h were systematically tested. To simulate *Xist* RNA-mediated silencing of *Tsix*, the *Tsix* promoter is assumed to be turned off by the *Xist* RNA. Since *Tsix* transcription is thought to induce a repressed chromatin state at the *Xist* promoter (Navarro et al., 2006; Sado et al., 2005), we further hypothesized that the *Xist* promoter transitions to the OFF-state when a PolII molecule transits in the antisense direction. The strength of *Tsix*-dependent repression of the *Xist* promoter is linked to the lifetime of the *Xist* promoter's OFF state, for which values ranging from tens of seconds to one hour were tested. Finally, since *Tsix* and *Xist* are transcribed in opposite directions across the same genomic region (~23kb) and RNA polymerases seem not to be able to bypass each other (Hobson et al., 2012), we assumed that one randomly chosen polymerase is removed from the DNA upon polymerase collision. This would therefore represent an additional and previously uncharacterized level of mutual repression of *Xist* and *Tsix*.

To investigate whether mutual repression of *Xist* and *Tsix* can maintain the mono-allelic XaXi state, we simulated the model for 8000 parameter sets, testing a wide range of values for the initiation rates of *Xist* and *Tsix,* k_X and k_T and the repression strength of the *Xist* promoter. All simulations assumed the presence of only a single XXA dose at the maintenance stage, i.e. after XCI (and down-regulation of XXA on the Xi) has occurred. Fluctuations can have a significant impact on the outcome of molecular processes in the presence of low numbers of molecules. In principle thus, fluctuations in PolII binding to the two promoters of *Tsix* and *Xist* in each single cell could affect the ability of the *Tsix*-mediated positive feedback loop to stabilize the Xa and Xi states. To take such fluctuations into account we use the stochastic Gillespie algorithm to simulate individual cells. With one chromosome starting from Xa (*Tsix* transcribed, *Xist* repressed) and one chromosome starting from Xi initial conditions (*Xist* expressed, *Tsix* silenced), 100 cells were simulated for each parameter set for 500 h (Fig. 2B+C). For ~50% of parameter sets high *Xist* expression from the Xi and low expression from the Xa was maintained in

all cells (example simulation in Fig. 2C), showing that mutual repression between *Xist* and *Tsix* can indeed stabilize the mono-allelic expression state of *Xist*.

We next asked whether all three mechanisms of mutual inhibition were required to stabilize the XaXi state. To this end we developed several reduced models with various combinations of polymerase collisions, *Xist* repression or *Tsix* silencing. Each model was simulated for the same parameter sets as the full model and the fraction of parameter sets that could maintain the XaXi state were assessed (Fig. 2D). This analysis revealed that at least two repressive mechanisms were required to maintain the mono-allelic state and that one of them had to be *Xist*-dependent silencing of the *Tsix* promoter. The central role played by *Xist*-mediated silencing can be attributed to the fact that the levels of a stable RNA such as *Xist* with a half-life of several hours (Sun et al., 2006) vary on much longer time scales than fast fluctuating transcription events. Therefore, RNA-mediated silencing is able to filter out high-frequency transcriptional noise and can thus stabilize the transcriptional state of the *Xist*-expressing chromosome reliably.

To further understand the requirements for maintenance of the mono-allelic state, we analyzed those parameter sets that were able to maintain the XaXi state. We found that the ratio of the *Xist* and *Tsix* initiation rates (k_X/k_T) played a central role, since the XaXi state was maintained for $k_X<k_T$ ($\log_2(k_X/k_T)<0$), while *Xist* tended to be up-regulated from the Xa for $k_X>k_T$ resulting in an XiXi state at the end of the simulation (Fig. 2E, example simulation in 2C). If we define an activation threshold as the k_X-to-k_T ratio above which at least one out of 100 cells up-regulates *Xist* from the Xa, we find that $k_X/k_T \approx 1$ at the threshold, with k_X being slightly lower than k_T (Fig. 2G, dotted line in Fig. 2F). A change in k_X (or k_T) across the threshold can shift the system between a regime where both the Xa and Xi states are maintained and a regime where the Xa is unstable and *Xist* is up-regulated (Fig. 2F). In the next section we will show that the cell must reside above the threshold to initiate *Xist* up-regulation at the onset of differentiation, and that the system should then shift below the threshold for maintenance of the mono-allelic state.

The model can reproduce mono-allelic *Xist* up-regulation

To address whether the model could explain how mono-allelic *Xist* expression is initially established, we further developed it to simultaneously take into account the XXA-mediated negative feedback as well as developmental regulation of *Xist* (Fig. 3A+B). To incorporate pluripotency factor-mediated repression of *Xist* (Navarro and Avner, 2010), we set the effective *Xist* initiation rate to $k_X^{eff} = 0.1 * k_X$ in the undifferentiated state. During differentiation, when pluripotency factors are down-regulated, we assumed $k_X^{eff} = q_{XA} \cdot k_X$, with $q_{XA} = 2$ reflecting the double XXA dose present. We further added

four additional parameters describing silencing and reactivation of XXA and *Tsix*, since these kinetics impact the dynamics of *Xist* up-regulation. The XXA silencing delay describes the time needed for its total disappearance, thus incorporating also RNA/protein degradation. Reactivation is assumed to occur if *Xist* happens to be down-regulated again after initiation of XCI, during the time window when silencing is still reversible (Wutz et al., 2000). Each parameter set that was found to be able to maintain the mono-allelic state in the previous section was combined with 500 values for the silencing and reactivation parameters for XXA and *Tsix* ranging from minutes to several days. We simulated 100 cells for 4 days, initiating from an XaXa state with double XXA dosage (Fig. 3B). Around 1% of the >1 Mio. parameter sets could indeed reproduce mono-allelic up-regulation of *Xist* (see example simulation in Fig. 3C), showing that the model can explain the random choice process of the inactive X.

To understand the prerequisites for mono-allelic up-regulation, we simulated the onset of XCI using the simplified models that were found to maintain the XaXi state in the previous section (cp. Fig. 2D). *Tsix*-dependent repression of *Xist* was found to be dispensable also for initiation of XCI, while RNA polymerase collisions across the *Xist/Tsix* overlapping region were strictly required (Fig. 3D, discussed in more detail below).

Using the simplified model where mutual repression of *Xist* and *Tsix* occurs through *Xist*-mediated silencing and polymerase collisions, we then asked which parameter sets allowed mono-allelic *Xist* up-regulation (described in detail in the supplemental material). While the network must reside below the activation threshold in the presence of a single XXA dose to maintain the XaXi state (Fig. 3E, grey), it must cross this threshold when a double XXA dose is present to allow *Xist* up-regulation during the initiation phase (Fig. 3E, yellow). Only parameter sets with a k_X-to-k_T ratio up to two-fold below the activation threshold in the presence of a single XXA dose are thus expected to traverse the threshold when a double dose is present. Compatibly, the k_X-to-k_T ratio of those parameter sets that could reproduce reliable mono-allelic *Xist* up-regulation was found between 0.4 and 0.8 just below the threshold at $k_X/k_T \approx 1$ (Fig. 3F, cp. Fig. 2G). In addition, the activation threshold must be rather sharp so that a relatively small two-fold change in k_X resulting from the silencing of one XXA copy during XCI can induce a switch from reliable up-regulation of *Xist* to reliable maintenance. Comparison of the reduced models revealed that such a sharp threshold is only generated, if polymerase collisions are taken into account (Fig. S1A-D), thus explaining why the model without collisions could not recapitulate the mono-allelic choice process (see above). The k_X-to-k_T ratio also controls the kinetics of the transitions between the *Xist*- and the *Tsix* expressing states (switch-ON/OFF). For higher k_X-to-k_T ratios, *Xist* up-regulation is faster and the *Xist* expressing state is more stable (see suppl. material). Since XXA silencing reduces k_X, this destabilizes the *Xist* expressing state if *Tsix* has not

yet been silenced. Therefore silencing of XXA and *Tsix* must occur on similar time scales in order to allow reliable mono-allelic *Xist* up-regulation (Fig. 3G).

To transition from a symmetric XaXa to an asymmetric XaXi state, a symmetry-breaking event is required, which can occur at different stages of the initiation of XCI and thereby result in alternative routes to the mono-allelic state (Fig. 3H). In one scenario, symmetry-breaking occurs when *Xist* is stochastically up-regulated from only one out of two alleles and the mono-allelic state is subsequently stabilized by rapid silencing of XXA and *Tsix* (Fig. 3H, left). Such direct mono-allelic up-regulation requires a slow and therefore highly variable switch-ON time of *Xist* combined with rapid silencing kinetics for XXA and *Tsix*, which will shift the system to the maintenance regime before up-regulation from the other X-chromosome occurs. In an alternative scenario where the switch-ON time is faster, *Xist* might be up-regulated from both chromosomes before silencing occurs (Fig. 3H, middle+right). In this case symmetry breaking can be achieved through mono-allelic silencing of XXA and *Tsix*, which will determine the choice of the inactive X. The other chromosome (Xa) will switch off *Xist* rapidly in the presence of only a single XXA dose, if *Tsix* has not been silenced (Fig. 3H, middle). In cases where the cell fails to achieve symmetry-breaking and both chromosomes are silenced, *Xist* transcription cannot be maintained because XXA is silenced on both chromosomes, which results in *Xist* down-regulation (Fig. 3H, right). Upon reactivation of *Tsix* and XXA the cell can then undertake a second attempt to reach the mono-allelic state. In fact, we found a large number of parameter sets that exhibit transient bi-allelic *Xist* up-regulation, but then reach a mono-allelic expression state in a very reliable fashion. Which of the routes is taken to achieve the mono-allelic state in the majority of cells is determined by the relative time scales of *Xist* up-regulation (Switch-ON) and XXA silencing (Fig. 3I).

In summary, the model can recapitulate mono-allelic up-regulation of *Xist* during differentiation for a set of parameter values, and it strictly depends on the presence of polymerase collisions. Furthermore, the mono-allelic state can be reached directly but also via transient bi-allelic expression, depending on the precise parameter values.

Xist interferes with elongation at the *Tsix* gene

Since the model predicts that mutual transcriptional interference of *Xist* and *Tsix* mediated by Polymerase collisions is required for a sharp activation threshold, we next set out to generate experimental support that antisense *Tsix/Xist* transcription indeed exerts a repressive effect on the level of transcriptional elongation. To this end we used several ES cell lines carrying the TX allele, where the endogenous *Xist* gene is controlled by a doxycycline inducible promoter, thus uncoupling *Xist* regulation from the transcriptional activity of *Tsix* (Fig. 4A). Upon *Xist* induction in the hybrid female ES cell

line TX1072 and an XO subclone of that line (Schulz et al., 2014) we quantified *Tsix* RNA produced by the TX allele by pyrosequencing, which allows allele-specific analysis, and by qPCR, respectively (primer positions in Fig. 5B). In both cell lines *Tsix* was barely affected by *Xist* induction upstream of the overlapping region (5'), but was strongly reduced by ~50% downstream of *Xist* (3') after 8 h of Doxycycline treatment (Fig. 4C). In addition spliced *Tsix* was also strongly reduced, since the splice acceptor site is close to the 3' end (Fig. 4C, bottom). These results show that *Xist* induction indeed interferes with *Tsix* elongation.

Due to the switch-like behavior of the locus, the model predicts that either *Xist* or *Tsix*, but not both are transcribed at a given time (Fig 3C, bottom). We thus quantified nascent transcription by RNA FISH in the male TXY cell line carrying the TX allele (Wutz et al., 2002) using intronic oligonucleotide-based probes. For *Tsix* we designed two different probes to detect transcription upstream of *Xist* (5') and within the overlapping region (3') (Fig. 4B). As predicted, transcription of *Xist* and *Tsix* was mutually exclusive in nearly all cells after one day of Doxycyline treatment (Fig. 4D). To be able to observe transcriptional interference independent of *Xist* RNA mediated silencing, we used the silencing deficient TXYΔA line carrying a deletion of the A-repeat of *Xist* (Wutz et al., 2002). Strikingly, almost complete *Tsix/Xist* exclusion in the overlapping region was observed also in this case (Fig. 4E). We next compared the signal intensity of the two Tsix probes at *Xist* transcribing (*Xist*+) and not transcribing (*Xist*-) alleles. In the TXY line both *Tsix* signals of the 3' and 5' probes were strongly reduced on the *Xist*+ alleles compared to *Xist*- alleles likely due to *Xist*-RNA mediated silencing of *Tsix*, while in TXYΔA cells the *Tsix* 5' region was barely affected compared to the 3' position (Fig. 4F). Thus we conclude that transcriptional interference perturbs transcriptional elongation at the *Xist/Tsix* antisense locus, as predicted by the model.

Transient bi-allelic *Xist* up-regulation during ES cell differentiation

Our model analysis showed that a single network architecture can generate different degrees of transient biallelic *Xist* expression. The decision as to whether a cell will undergo direct mono-allelic up-regulation or follow a route via transient bi-allelic expression depends on which reaction occurs first: Silencing or up-regulation of *Xist* from the second allele (Fig. 3H bottom, reaction 3a vs 2). If one could artificially accelerate *Xist* up-regulation from one allele, this would prolong the time before *Xist* is up-regulated from the other allele. As a result, the switch-ON-to-silencing ratio would be increased and the extent of transient bi-allelic expression reduced (cp. Fig. 3I). To test this prediction experimentally, we again used the female TX1072 cell line, where *Xist* up-regulation from one allele can be accelerated by doxycyline addition (Fig. 5A). Doxycyline treatment one day before the onset of differentiation resulted in *Xist* up-

regulation in 50-70% of cells as judged by RNA FISH (Fig. 5B+C). As predicted by the model, the extent of transient bi-allelic expression was significantly reduced from ∼20% in control cells to <5% in doxycyline treated cells (Fig. 5C). Speeding up *Xist* up-regulation can thus indeed modulate the extent of bi-allelic *Xist* expression.

The second prediction that we aimed to test was that transient bi-allelic expression could be resolved to a mono-allelic state (Fig. 3H, middle/right). We set up an experimental system to artificially increase the extent of bi-allelic *Xist* up-regulation. To this end, we deleted the *DXPas34* enhancer of *Tsix* from the Castaneus (Cast) allele in the TX1072 ESC line (Fig. 5D), which results in preferential *Xist* up-regulation from the mutant chromosome (Lee and Lu, 1999). We differentiated the cells for 48h to trigger up-regulation of *Xist* from the Cast allele and then added Doxycycline to also induce *Xist* from the B6 chromosome (Fig. 5E). In this way, we could increase the amount of bi-allelically expressing cells from ∼10% to ∼30% (Fig. 5F). Since *Xist* expression from the B6 chromosome is maintained by Doxycyline, the cells are predicted to down-regulate *Xist* from the Cast chromosome to resolve the bi-allelic expression state. To quantify *Xist* expression in an allele-specific way, we used the Illumina targeted expression assay to perform amplicon-sequencing of SNPs on cDNA. This showed that *Xist* from the Cast chromosome was significantly down-regulated 48h after Doxycycline treatment compared to the untreated control (Fig. 5G, light green). To distinguish whether *Xist* up-regulation had indeed been reversed or whether bi-allelically *Xist* expressing cells were just counter-selected, we performed Immuno-RNA FISH for *Xist*, *Huwe1* (an X-linked gene) and H3K27me3, which is recruited to the chromosome following *Xist* RNA coating (Augui et al., 2011). We identified chromosomes that had ceased to express *Xist* and expressed *Huwe1*, but were still enriched for H3K27me3 (as this mark is lost more slowly from X chromatin), even in the absence of an *Xist* signal and named these Xa* (scheme in Fig. 5E, example image Fig. 5I). Quantification of cells that had reverted from a bi-allelic to a mono-allelic state (Xa*Xi) revealed that these were rarely observed after 4 days of differentiation without Doxycyline (<5%), but constituted >10% of cells upon bi-allelic induction of *Xist* (Fig. 5H). We thus conclude that a bi-allelic *Xist* expression state can indeed be resolved by down-regulation of one *Xist* allele.

Bi-allelic *Xist* expression in mouse embryos

Our model analysis has shown that the same regulatory network can generate different degrees of transient biallelic *Xist* up-regulation. The fact that bi-allelic expression has not been reported for mouse embryos, but is frequently observed in humans and rabbits (Sado and Sakaguchi, 2013) might thus be due to potentially different time scales of *Xist* up-regulation and XXA silencing in those species. However, the model predicts that a very low level of bi-allelic expression (<5%) would require the switch-ON time of *Xist* to

be at least 5 to 10 times slower than XXA silencing (Fig. 3I). If we take into account that even for rapidly silenced genes the silencing delay is in the range of hours, the switch-ON time should be longer than 10h. Such slow dynamics of *Xist* up-regulation however would be difficult to reconcile with the fact that the transition to the mono-allelic state occurs within 24h between E4.5 and E5.5 of development (Mak et al., 2004; Okamoto et al., 2004; Sakata et al., 2017). We therefore hypothesized that also in mouse embryos a fraction of cells should up-regulate *Xist* bi-allelically and set out to study the *Xist* expression pattern *in vivo* in the E5.0 epiblast where random XCI is first initiated (Fig. 6A). RNA FISH indeed revealed that 15-20% of epiblast cells in each embryo exhibited two *Xist* clouds (Fig. 6B-D). From these data we conclude that transient bi-allelic *Xist* expression also occurs during mouse development, but to a lesser extent than in rabbits or humans. This can be explained in the framework of the proposed model, if we assume that either *Xist* is up-regulated more slowly or XXA is silenced more rapidly in mice compared to the other species.

The model can explain X-inactivation mutant phenotypes and aneuploidies

To further validate the model, we simulated a series of mutant cell lines and X aneuploidies that have been described in previous studies. For the model where mutual repression of *Xist* and *Tsix* is mediated by *Xist*-RNA dependent silencing and collisions (cp. Fig. 3D) we selected 100 parameter sets that reproduced *Xist* up-regulation in embryonic stem cells with respect to the timing of *Xist* up-regulation (<48h), the expression level of *Xist* (200-600 molecules) and the extent of transient bi-allelic expression (<20%). Using again the stochastic Gillespie algorithm for each parameter set 100 cells were simulated for each of four genotypes: wildtype, heterozygous and homozygous *Tsix* mutant and heterozygous *Xist* mutant cells (Fig. 7A-D). In our simulations, each chromosome in wildtype cells is inactivated with an equal probability such that 50% of cells will express *Xist* from one or the other X-chromosome (Fig. 7A, bottom). In agreement with experimental observations, a heterozygous *Tsix* mutation, simulated by setting the *Tsix* initiation rate k_T to 0 results in non-random X-inactivation of the mutant X-chromosome (Fig. 7B, bottom) (Lee and Lu, 1999). A heterozygous *Xist* deletion by contrast (simulated as $k_X=0$) results in complete skewing towards the wildtype allele, but nevertheless most cells up-regulated *Xist* after 4 days of differentiation (Fig. 7D, bottom). For homozygous *Tsix* mutants, 'chaotic' X-inactivation has been described with a mixture of cells inactivating one or two X-chromosomes (Lee 2005). In our simulations such a mutation would result in *Xist* oscillations, where *Xist* is turned on bi-allelically, which will result in complete XXA silencing and *Xist* down-regulation, followed by another round of bi-allelic up-regulation (Fig. 7C, top). In

agreement with the experimental phenotype these simulations indeed show a strongly increased fraction of bi-allelically expressing cells (Fig. 7C, bottom).

We also compared the kinetics of *Xist* up-regulation, since a heterozygous *Tsix* mutation had been shown to accelerate XCI, while an *Xist* mutation had slowed down XCI in a previous study (Monkhorst 2008). To test this, we calculated the half time of *Xist* up-regulation ($T_{1/2}$) where 50% of cells would have turned on *Xist* (example in Fig. 7E) and compared this value between mutant and wildtype cells. Indeed for all parameter sets tested, a *Tsix* mutation would reduce the half time of *Xist* up-regulation while it would be increased in *Xist* mutant cells (Fig. 7F).

In the next step, we tested whether the model could explain the phenotype observed for different X aneuploidies. It is known that in diploid cells (2n), all X chromosomes except one will be inactivated ultimately (Brown et al., 1992). If we assume that each additional X chromosome produces an additional dose of XXA and thereby increases the *Xist* initiation rate accordingly (Fig. 7G), all parameter sets correctly predict no *Xist* expression in male and XO cells and bi- and tri-allelic *Xist* expression in X-chromosome trisomies and – tetrasomies, respectively (Fig. 7H). This can be explained by the fact that the Xa state remains unstable as long as more than one XXA dosage is present (Fig. 7G, yellow area), which will result in inactivation of more X chromosomes until only one active X remains.

While the model can correctly predict the behavior of a diploid cell (2n) with four X chromosomes (X tetrasomy), it is less straight forward to explain tetraploid cells (4n), which also contain four X chromosomes, but only inactivate two of them (Monkhorst et al., 2008). To simulate tetraploid cells, we assumed that the two-fold increase in genome size would result in a two-fold bigger nuclear volume (Henery et al., 1992). Although the number of XXA molecules would double due to the presence 4 XXA loci, the two-fold dilution due to the larger volume would compensate this increase, such that the concentration of the X-linked activator would be comparable in diploid and tetraploid cells. As a result, a tetraploid cell with two Xa (2xXXA) will reside in the maintenance regime, such that an XiXiXaXa state would be stable (Fig. 7I). It is more difficult to imagine however, how this bi-allelic expression state could be reached during differentiation. While the Xa is unstable with 4x XXA, this is not necessarily the case for 3x XXA (Fig. 7I). When we tested all parameter sets that could explain mono-allelic *Xist* expression in diploid cells, only a subset of them resulted in bi-allelic *Xist* expression in tetraploid cells (Fig. 7J). However, when we selected only those parameter sets where the Xa state was unstable for a triple XXA dose (Fig. 7I, blue arrows), they could indeed reproduce bi-allelic *Xist* up-regulation in >70% of cells (Fig. 7K). The reason that it appears to be more difficult to reach the bi-allelic state in tetraploid cells in a reliable fashion than the mono-allelic state in diploid cells, is that it is more challenging to distinguish between 2x and 3x XXA which is only a 50% increase, compared to the

distinction between 1x and 2x XXA in diploid cells, which is a 100% increase. As a consequence we do not find any parameter set were bi-allelic *Xist* up-regulation would occur in 100% of tetraploid cells. Those cells that fail to up-regulate *Xist* from exactly two chromosomes might subsequently be counterselected, since abnormal X-dosage upon failure to undergo XCI has been shown to result in genome-wide transcriptional misregulation (Borensztein et al., 2017).

Taken together, we have shown that parameter sets that can reproduce mono-allelic *Xist* up-regulation in diploid female cells can also correctly predict *Xist* expression patterns in a series of *Xist* and *Tsix* mutant situations, as well as the different XCI patterns in X tri- and tetrasomies and bi-allelic *Xist* up-regulation in tetraploid cells.

Discussion

We present the first mechanistic model that can explain initiation and maintenance of mono-allelic *Xist* expression and can correctly reproduce the *Xist* patterns observed in several mutant cell lines, in X tri- and tetrasomies and in tetraploid cells. While a previous modeling study had shown that stochastic *Xist* up-regulation by a dose-sensitive X-linked XCI activator together with a negative feedback loop could reproduce mono-allelic *Xist* expression, it did not address how a postulated threshold could be generated on the molecular level and how *Xist* expression can be maintained (Monkhorst et al., 2009). We show that initial maintenance of the alternative expression states of the Xa and Xi requires a *cis*-acting positive feedback loop, at least until they are locked in by epigenetic mechanisms such DNA methylation (Augui et al., 2011). In mice, this can be mediated by mutual repression of *Xist* and *Tsix*, which form a bistable switch and thereby generate the previously postulated threshold. Above the threshold *Xist* can is up-regulated and below both *Xist*-expressing and non-expressing states are maintained. Upon down-regulation of pluripotency factors at the onset of differentiation, cells are licensed to up-regulate *Xist*. Due to XXA silencing, the *Xist* initiation rate then drops below the threshold where the system is bistable and two alternative *Xist* expression states can be maintained. We provide evidence that transcriptional interference, potentially mediated by polymerase collisions, can occur in the 23kb region across which *Xist* and *Tsix* are transcribed in opposite directions. Taking this mechanism into account, the threshold is sharp enough to reliably distinguish between a single and a double dose of an X-linked activator. The *Xist*/*Tsix* locus is thus an example of how antisense transcription, which is prevalent in many organisms, might control decision-making processes also at other loci, as suggested by the finding that genes associated with antisense transcription exhibit increased expression variability (Xu et al., 2011).

Initial up-regulation of *Xist* occurs independently on each chromosome, and information about the state of the other *Xist* locus is only exchanged through silencing of the *trans*-acting *Xist* activator. The model predicts indeed that bi-allelic *Xist* up-regulation occurs in a subset of cells, if initiation of XCI is to be completed within a physiologic time frame. When analyzing mouse embryos right at the onset of random XCI at E5.0, we indeed observe ~20% bi-allelic *Xist* expression, which until now had not been described in mice. In differentiating ES cells by contrast highly variable levels of bi-allelic *Xist* expression between <1% and 15% have been reported (Augui et al., 2007; Guyochin et al., 2014; Lee, 2005; Monkhorst et al., 2008). Such variability can probably be attributed to different genetic backgrounds and differentiation protocols, which are expected to affect the activity of transcription factors controlling *Xist* and *Tsix* and the silencing kinetics of X-linked genes (potentially including XA factors), which have been shown to vary based on genetic background (Borensztein et al., 2017). Such differences are expected to modulate the extent of bi-allelic *Xist* expression, which is sensitive to the relative time scales of *Xist* up-regulation and gene silencing.

Xist's ability to silence X-linked genes is crucial for the positive feedback, where *Tsix* must be silenced to sustain *Xist* expression, and for the negative feedback, where silencing of the *Xist* activator prevents bi-allelic up-regulation. Depending on the precise parameter regime, the model would thus predict that either *Xist* expression cannot be sustained in the absence of silencing or it will be up-regulated biallelically. A failure to up-regulate *Xist* has indeed has been observed in mouse embryos carrying a deletion of the A-repeat (ΔA), which is required for *Xist's* silencing function, but was interpreted as a disruption of an *Xist* enhancer element (Hoki et al., 2009). *Xist* up-regulation was restored when the ΔA allele was put under control of a strong beta-actin promoter, which can override *Tsix*-mediated repression and resulted in sustained bi-allelic *Xist* expression at E7.5 (Sakata et al., 2017). In this genotype the central role of silencing in mediating the negative feedback to prevent bi-allelic expression becomes evident. While such a feedback has been proposed to ensure mono-allelic *Xist* up-regulation (Monkhorst et al., 2008), we now present evidence that bi-allelic up-regulation is initially reversible and that the negative feedback can resolve it to a mono-allelic state. Through forcing bi-allelic *Xist* up-regulation using an inducible system we observe a significant fraction of cells, where *Xist* is expressed from one allele, but both X-chromosomes have accumulated H3K27me3, suggesting that *Xist* had initially been up-regulated from both chromosomes, but has been reverted to the mono-allelic state. Initial bi-allelic *Xist* up-regulation might be the ancestral route to mono-allelic *Xist* expression, which is less frequently used in mice than in other mammals.

Since initiation of XCI has most extensively been studied in the mouse, the model we present describes regulation of the murine *Xist* gene. It can however also capture some

aspects of *Xist* regulation observed in other mammals. Since the prominent role played by *Tsix* in mice has not been shown for other species (Sado and Sakaguchi, 2013), the *cis*-acting positive feedback loop might be implemented in a different way in other mammals. It could be mediated by another repressive *cis*-acting locus or at the level of chromatin readers and writers as shown for the *flc* locus in Arabidopsis (Angel et al., 2011; Dodd et al., 2007). The prediction of transient bi-allelic *Xist* expression, however, is independent of the exact implementation of the positive feedback and can thus explain the different *Xist* patterns found in early embryos from rabbits and humans (Okamoto et al., 2011). In rabbits, bi-allelic *Xist* expression is observed in up to 50% of cells and is resolved to a mono-allelic state within 24h, a scenario that can be reproduced by our model. In early human embryos, XIST is expressed from both chromosomes in most cells at the blastocyst stage, but fail to induce gene silencing (Okamoto et al., 2011). Instead dampening of expression from both X chromosomes might enable some degree of dosage compensation (Petropoulos et al., 2016). Indeed in our model bi-allelic XIST expression could persist, if the XIST activator is not sufficiently silenced. Recent work using naive human pluripotent stem cells suggests that XIST might be down-regulated again from both chromosomes before random X-inactivation is initiated (Sahakyan et al., 2017). Since culture conditions that would allow random X inactivation *in vitro* have not yet been identified it remains to be seen whether human cells will also transit through a transient bi-allelic state, as seen in rabbit and mouse embryos. Nevertheless, the present study reveals that the regulatory principles employed by different mammalian species might be less diverse than previously thought and that the different routes to the mono-allelic state could be attributed to quantitative differences in reaction rates rather than qualitative differences in the network architecture.

Author contributions

Acknowledgements

fellowship (LT000597/2010-L) to E.G.S., a grant-in-aid from MEXT and JST-ERATO to I.O. and M.S., JSPS KAKENHI Grant Number JP25291076 to I.O., the Max-Planck Research Group Leader program and and the German Ministry of Science and Education (BMBF) through the grant E:bio Module III - Xnet. V.M. is supported by the DFG (GRK1772: Computational Systems Biology).

References

Angel, A., Song, J., Dean, C., and Howard, M. (2011). A Polycomb-based switch underlying quantitative epigenetic memory. Nature *476*, 105–108.

Augui, S., Filion, G.J., Huart, S., Nora, E.P., Nora, E., Guggiari, M., Maresca, M., Stewart, A.F., and Heard, E. (2007). Sensing X chromosome pairs before X inactivation via a novel X-pairing region of the Xic. Science *318*, 1632–1636.

Augui, S., Nora, E.P., and Heard, E. (2011). Regulation of X-chromosome inactivation by the X-inactivation centre. Nature Reviews Genetics *12*, 429–442.

Bacher, C.P., Guggiari, M., Brors, B., Augui, S., Clerc, P., Avner, P., Eils, R., and Heard, E. (2006). Transient colocalization of X-inactivation centres accompanies the initiation of X inactivation. Nat Cell Biol *8*, 293–299.

Barakat, T.S., Loos, F., van Staveren, S., Myronova, E., Ghazvini, M., Grootegoed, J.A., and Gribnau, J. (2014). The Trans-Activator RNF12 and Cis-Acting Elements Effectuate X Chromosome Inactivation Independent of X-Pairing. Molecular Cell *53*, 965–978.

Borensztein, M., Syx, L., Ancelin, K., Diabangouaya, P., Picard, C., Liu, T., Liang, J.-B., Vassilev, I., Galupa, R., Servant, N., et al. (2017). Xist-dependent imprinted X inactivation and the early developmental consequences of its failure. Nat Struct Mol Biol *24*, 226–233.

Brown, C.J., Hendrich, B.D., Rupert, J.L., Lafrenière, R.G., Xing, Y., Lawrence, J., and Willard, H.F. (1992). The human XIST gene: analysis of a 17 kb inactive X-specific RNA that contains conserved repeats and is highly localized within the nucleus. Cell *71*, 527–542.

Di Tian, Sun, S., and Lee, J.T. (2010). The Long Noncoding RNA, Jpx, Is a Molecular Switch for X Chromosome Inactivation. Cell *143*, 390–403.

Dodd, I.B., Micheelsen, M.A., Sneppen, K., and Thon, G. (2007). Theoretical analysis of epigenetic cell memory by nucleosome modification. Cell *129*, 813–822.

Giorgetti, L., Galupa, R., Nora, E.P., Piolot, T., Lam, F., Dekker, J., Tiana, G., and Heard, E. (2014). Predictive polymer modeling reveals coupled fluctuations in chromosome conformation and transcription. Cell *157*, 950–963.

Guyochin, A., Maenner, S., Chu, E.T.-J., Hentati, A., Attia, M., Avner, P., and Clerc, P. (2014). Live cell imaging of the nascent inactive X chromosome during the early differentiation process of naive ES cells towards epiblast stem cells. PLoS ONE *9*, e116109.

Heard, E., Mongelard, F., Arnaud, D., and Avner, P. (1999). Xist yeast artificial chromosome transgenes function as X-inactivation centers only in multicopy arrays and not as single copies. Molecular and Cellular Biology *19*, 3156–3166.

Henery, C.C., Bard, J.B., and Kaufman, M.H. (1992). Tetraploidy in mice, embryonic cell number, and the grain of the developmental map. Developmental Biology *152*, 233–241.

Hobson, D.J., Wei, W., Steinmetz, L.M., and Svejstrup, J.Q. (2012). RNA Polymerase II Collision Interrupts Convergent Transcription. Molecular Cell.

Hoki, Y., Kimura, N., Kanbayashi, M., Amakawa, Y., Ohhata, T., Sasaki, H., and Sado, T. (2009). A proximal conserved repeat in the Xist gene is essential as a genomic element for X-inactivation in mouse. Development *136*, 139–146.

Jonkers, I., Barakat, T.S., Achame, E.M., Monkhorst, K., Kenter, A., Rentmeester, E., Grosveld, F., Grootegoed, J.A., and Gribnau, J. (2009). RNF12 Is an X-Encoded Dose-Dependent Activator of X Chromosome Inactivation. Cell *139*, 999–1011.

Lee, J.T. (2005). Regulation of X-Chromosome Counting by Tsix and Xite Sequences. Science *309*, 768–771.

Lee, J.T., and Lu, N. (1999). Targeted mutagenesis of Tsix leads to nonrandom X inactivation. Cell *99*, 47–57.

Mak, W., Nesterova, T.B., de Napoles, M., Appanah, R., Yamanaka, S., Otte, A.P., and Brockdorff, N. (2004). Reactivation of the paternal X chromosome in early mouse embryos. Science *303*, 666–669.

Monkhorst, K., de Hoon, B., Jonkers, I., Mulugeta Achame, E., Monkhorst, W., Hoogerbrugge, J., Rentmeester, E., Westerhoff, H.V., Grosveld, F., Grootegoed, J.A., et al. (2009). The Probability to Initiate X Chromosome Inactivation Is Determined by the X to Autosomal Ratio and X Chromosome Specific Allelic Properties. PLoS ONE *4*, e5616.

Monkhorst, K., Jonkers, I., Rentmeester, E., Grosveld, F., and Gribnau, J. (2008). X Inactivation Counting and Choice Is a Stochastic Process: Evidence for Involvement of an X-Linked Activator. Cell *132*, 410–421.

Navarro, P., and Avner, P. (2010). An embryonic story: Analysis of the gene regulative network controlling Xist expression in mouse embryonic stem cells. Bioessays *32*, 581–588.

Navarro, P., Page, D.R., Avner, P., and Rougeulle, C. (2006). Tsix-mediated epigenetic switch of a CTCF-flanked region of the Xist promoter determines the Xist transcription program. Genes & Development *20*, 2787–2792.

Nicodemi, M., and Prisco, A. (2007). Symmetry-Breaking Model for X-Chromosome Inactivation. Phys. Rev. Lett. *98*.

Okamoto, I., Otte, A.P., Allis, C.D., Reinberg, D., and Heard, E. (2004). Epigenetic dynamics of imprinted X inactivation during early mouse development. Science *303*, 644–649.

Okamoto, I., Patrat, C., Thépot, D., Peynot, N., Fauque, P., Daniel, N., Diabangouaya, P.,

Wolf, J.-P., Renard, J.-P., Duranthon, V., et al. (2011). Eutherian mammals use diverse strategies to initiate X-chromosome inactivation during development. Nature *472*, 370–374.

Petropoulos, S., Edsgärd, D., Reinius, B., Deng, Q., Panula, S.P., Codeluppi, S., Plaza Reyes, A., Linnarsson, S., Sandberg, R., and Lanner, F. (2016). Single-Cell RNA-Seq Reveals Lineage and X Chromosome Dynamics in Human Preimplantation Embryos. Cell *165*, 1012–1026.

Sado, T., and Sakaguchi, T. (2013). Species-specific differences in X chromosome inactivation in mammals. Reproduction *146*, R131–R139.

Sado, T., Hoki, Y., and Sasaki, H. (2005). Tsix silences Xist through modification of chromatin structure. Developmental Cell *9*, 159–165.

Sahakyan, A., Kim, R., Chronis, C., Sabri, S., Bonora, G., Theunissen, T.W., Kuoy, E., Langerman, J., Clark, A.T., Jaenisch, R., et al. (2017). Human Naive Pluripotent Stem Cells Model X Chromosome Dampening and X Inactivation. Cell Stem Cell *20*, 87–101.

Sakata, Y., Nagao, K., Hoki, Y., Sasaki, H., Obuse, C., and Sado, T. (2017). Defects in dosage compensation impact global gene regulation in the mouse trophoblast. Development *144*, 2784–2797.

Schulz, E.G., Meisig, J., Nakamura, T., Okamoto, I., Sieber, A., Picard, C., Borensztein, M., Saitou, M., Blüthgen, N., and Heard, E. (2014). The Two Active X Chromosomes in Female ESCs Block Exit from the Pluripotent State by Modulating the ESC Signaling Network. Cell Stem Cell *14*, 203–216.

Sun, B.K., Deaton, A.M., and Lee, J.T. (2006). A Transient Heterochromatic State in Xist Preempts X Inactivation Choice without RNA Stabilization. Molecular Cell *21*, 617–628.

Wutz, A., Wutz, A., and Jaenisch, R. (2000). A shift from reversible to irreversible X inactivation is triggered during ES cell differentiation. Molecular Cell *5*, 695–705.

Wutz, A., Rasmussen, T.P., and Jaenisch, R. (2002). Chromosomal silencing and localization are mediated by different domains of Xist RNA. Nature Genetics *30*, 167–174.

Xu, N. (2006). Transient Homologous Chromosome Pairing Marks the Onset of X Inactivation. Science *311*, 1149–1152.

Xu, Z., Wei, W., Gagneur, J., nster, S.C.-M.U., Smolik, M.L.O., Huber, W., and Steinmetz, L.M. (2011). Antisense expression increases gene expression variability and locus interdependency. Mol. Syst. Biol. *7*, 1–10.

Figure Legends

Figure 1: Comparison of alternative model structures

(A) Four model structures are compared. (B-D) Three different simulations, initiating from an XaXi (B), XiXi (C) states in female cells and from an Xi state in male cells (D). A scheme (right) and representative simulations (ODE) of *Xist* levels (left) are shown. (E) 1000 parameter sets were tested for each model. The percentage of sets where the XaXi state is stable (1) and the XiXi state is unstable (2) and the Xi state in male cells is unstable (3) are shown.

Figure 2: Mutual repression of *Xist* and *Tsix* can maintain the XaXi state

(A-B) Schematic representation of the mathematical model (A) and the simulation (B) shown in C-G to test whether mutual repression of *Xist* (green) and *Tsix* (blue) can maintain the Xi state (*Xist* transcribed, *Tsix* silenced) on one chromosome and the Xa state (*Xist* repressed, *Tsix* transcribed) on the other chromosome in the presence of a single XXA dose. (C) Stochastic simulation of *Xist* expression in one cell from the two chromosomes (light and dark green) for two example parameter sets. (D) Percentage of parameter sets that maintain the XaXi state in >99% cells for the network shown in (A) and several reduced versions with only one or two repressive mechanisms. (E) The percentage of parameter sets that maintain the XaXi state (black) and that transition to an XiXi state (grey) for different k_X-to-k_T ratios. (F) For an example parameter set (k_T=113 h^{-1}, $t_{1/2}^{repr}$ =0.7 h) mean and standard deviation of *Xist* expression from the chromosomes that initiated as Xa (light green) and Xi (dark green), respectively, is shown for different values of k_X. The dotted line indicates the k_X threshold value, above which the Xa state becomes unstable (<99% stable) (G) The distribution of the k_X/k_T ratio at the activation threshold in F for all parameter sets.

Figure 3: The model can reproduce mono-allelic *Xist* up-regulation.

(A+B) Schematic representation of the network and simulation scheme, initiating from the XaXa state in undifferentiated cells where *Xist* is repressed by pluripotency factors (PP) and *Tsix* (blue) and XXA (orange) are transcribed. (C) Example simulation of *Xist* up-regulation in one cell: (top) *Xist* levels expressed from each chromosome (light and dark green) and (bottom) number of Pol II transcribing *Xist* (green) and *Tsix* (blue) or both (black) in a 10-minute time window at the chromosome that up-regulates *Xist*. (D) The percentage of parameter sets that initiated mono-allelic *Xist* up-regulation as in (C) in >99% cells for the full model and 2 reduced models (cp. Fig. 2A+D). (E) Schematic diagram of the stability of Xa and Xi (see Fig. 2G) as a function of k_X indicating how k_X is modulated by pluripotency factors (grey, repression) and XXA (orange, activation). (F-I)

Analysis of the simulation performed for the reduced model without *Xist* repression. (F) Distribution of the k_X-to-k_T ratio within all parameter sets that maintain the XaXi state (black) and within the subset that allow mono-allelic *Xist* up-regulation (grey). (G) Heatmap showing the percentage of parameter sets that allow mono-allelic *Xist* up-regulation for different combinations of the silencing delays of *Tsix* and XXA. (H) Example simulations of *Xist* levels (top) and the *Tsix* and XXA promoter states (middle) for each X-chromosome (light vs dark colors) in single cells. (bottom) Schematic representation of how k_X (X-axis) and *Xist* levels (Y axis) change along different routes to the XaXi state due to (1) differentiation, (2) *Xist* up-regulation, mono-allelic (3a) or bi-allelic (3b) XXA silencing and (4) switch-OFF before silencing in presence of a single XXA dose. (I) The maximal fraction of cells with bi-allelic *Xist* expression observed during the simulation as a function of the the ratio of switch-ON time (first time point, when >10 *Xist* molecules have been produced) and XXA silencing delay. Three example simulations are shown.

Figure 4: *Xist* interferes with *Tsix* elongation

(A) The TX allele carries a Doxycycline inducible promoter driving the endogenous *Xist* gene and was used to investigate whether *Xist* transcription would interfere with *Tsix* elongation in (C-F). (B) Position of primers and probes used in (C-F). (C) TX 1072 XX (top) and TX 1072 XO ESCs (bottom) were treated with docycyline for 8 h and *Tsix* transcription from the TX allele was assessed by pyrosequencing (XX) or qPCR (XO) at different position within the *Tsix* gene. Mean and standard deviation of three independent experiments is shown. (D-E) TXY (D) and TXY ΔA (E) ESCs were treated with Doxycyline for 24 hours and nascent transcription of *Xist* and *Tsix* (5' and 3') was assessed by RNA FISH (probe positions in B). Example images and quantification (right) of 245 (D) and 422 cells (E) is shown. Grey lines indicate the detection threshold estimated from negative control regions. (F) Cumulative distribution of *Tsix* signal intensity at *Xist*+ (green) and *Xist*- alleles (black) in TXY (left) and TXYΔA (right). For (D-F) one out of two experiments is shown.

Figure 5: Bi-allelic *Xist* up-regulation can be resolved

(A-C) Premature *Xist* up-regulation by Doxycyline treatment of TX1072 cells (A) one day before differentiation (B). Cells expressing *Xist* from one (left) or two chromosomes (right) were quantified by RNA-FISH (n>80). (D-I) Bi-allelic *Xist* up-regulation is artificially induced by treating TXdT1C6 cells (D) with Doxycyline after 48h of differentiation. (E) The model predicts *Xist* down-regulation from the Cast chromosome, potentially transitioning through an Xa* state, where H3K27me3 (red) is still enriched, while *Xist* (green) has already been down-regulated. (F) The *Xist* expression pattern at different time points after Dox addition as assessed by RNA FISH (n>100). (G) Allele-

specific analysis of *Xist* expression by Illumina targeted expression assay at different time points after Dox treatment. (H-I) Immunofluorescence followed by RNA-FISH to detect *Xist*, H3K27me3 and the nascent transcript of the X-linked gene Huwe1 48h after Dox induction (n>120). Three states were quantified (XaXi, Xa*Xi, XiXi) as shown in the example image (I). Mean and standard deviation of 3 independent experiments are shown. *p<0.05 in two-sample paired (C,F) or one-sample (G) T-test

Figure 6: Bi-allelic *Xist* expression in E5.0 embryos.

(A) Mono-allelic *Xist* up-regulation occurs between E4.5 and E5.5 of mouse development. (B-C) *Xist/Tsix* RNA FISH (green) and Dapi staining (blue) of female epiblast cells at E5.0 of embryogenesis. Example cells with 0,1 and 2 *Xist* clouds are marked and enlarged in (C). (D) Quantification of the number of cells in the epiblast with 0, 1 or 2 *Xist*-coated chromosomes for 15 female embryos.

Figure 7: *Xist/Tsix* mutants and X-aneuploidies

(A-D) Simulations of *Xist/Tsix* mutant cell lines (top). Representative simulation of *Xist* levels produced by the wildtype (black) and mutant (red) chromosomes of a single cell (upper middle) and by 100 cells (lower middle). Boxplot showing the percentage of cells expressing *Xist* mono-allelically from wildtype or mutant X or bi-allelically for all simulated parameter sets (bottom). (E-F) *Xist* up-regulation is accelerated in *Tsix$^{+/-}$* and delayed in *Xist$^{+/-}$* cells. Representative simulation (E) and the distribution of the change of half time ($\Delta T_{1/2}$) in the mutant genotypes (F). (G) Schematic diagram of the stability of Xa and Xi as a function of k_X indicating how different doses of XXA modulate k_X. (H) The percentage of cells with different Xi patterns for 100 parameter sets after 4 days of simulation for cells with 1,2,3 or 4 X-chromosomes. (I) Schematic diagram of the stability of Xa and Xi as a function of k_X indicating how different doses of XXA in diploid (2n) and tetraploid (4n) cells modulate k_X, assuming that a doubling of the nuclear volume in tetraploid cells will result in a two-fold XXA dilution. (J+K) The percentage of cells with different Xi patterns after 4 days of simulation of tetraploid cells for all parameter sets (J) or for those sets (blue in I), where a triple XXA dose resides in the upregulation regime (K).

Supplemental Figure Legends

Figure S1

(A-D) The simulations carried out to investigate under which conditions the full model and the reduced model without polymerase collisions could maintain the mono-allelic state were compared (see main Fig. 2 and supplemental material). (A+B) For an example parameter set (k_T=113 h^{-1}, $t_{1/2}^{repr}$ =0.7 h) mean and standard deviation of *Xist* expression from the chromosomes that initiated as Xa (light green) and Xi (dark green), respectively, is shown for different values of k_x for the full model (A) and the reduced model without collisions (B). The vertical lines indicate the k_X threshold value, above which >1 (red) or >99 (grey) out of 100 cells up-regulate *Xist* from the Xa. (C+D) The parameter regimes where the XaXi state is maintained (grey) or *Xist* is up-regulated from the Xa (yellow) in >99 out of 100 cells are show in the k_X/k_T space for the Full model (C) and the reduced model without collisions (D). Red and grey lines indicate the activation threshold as in (A+B).

Figure 1   *Mutzel et al.*
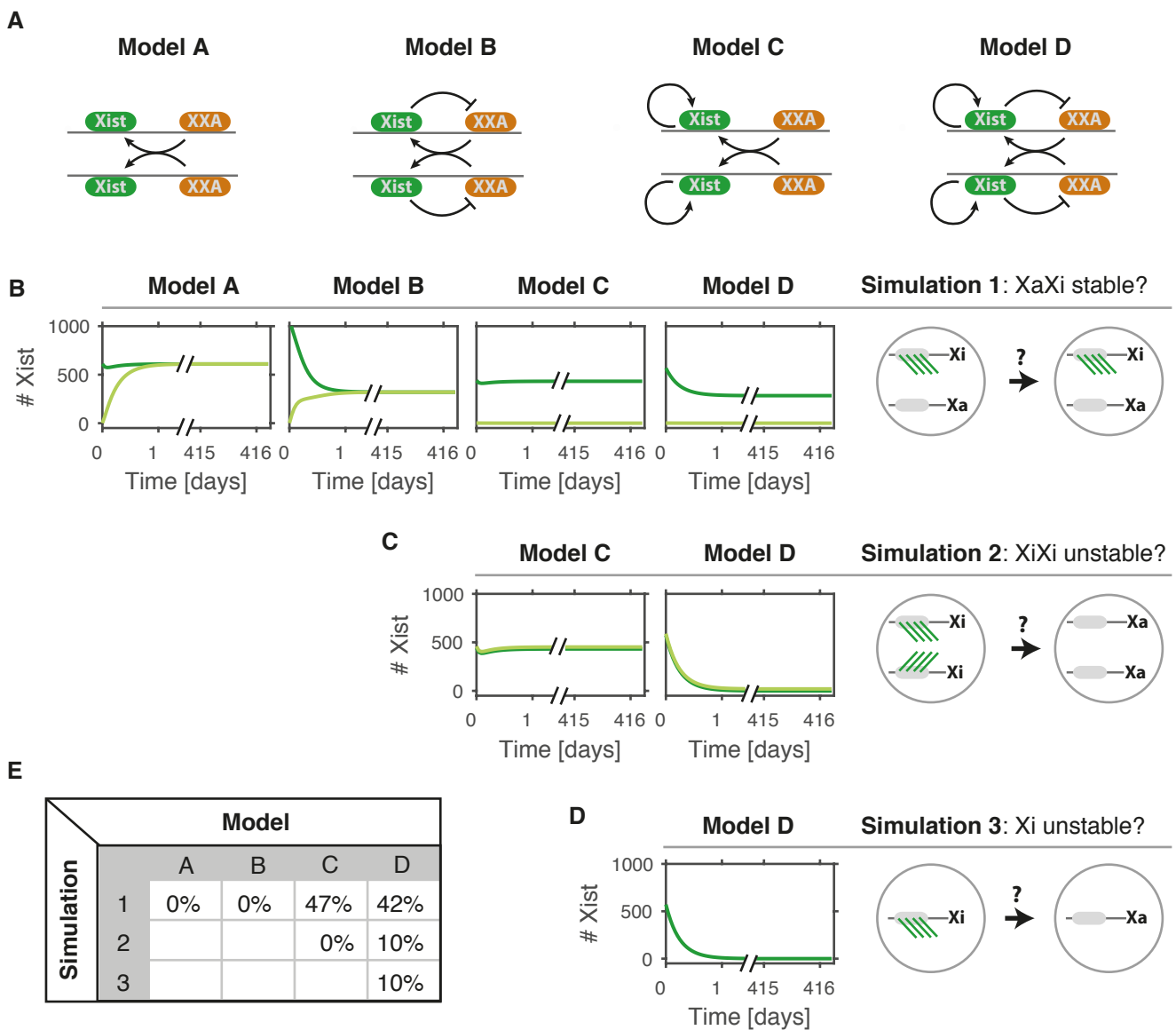
Figure 1: Comparison of alternative model structures
(A) Four model structures are compared. (B-D) Three different simulations, initiating from an XaXi (B), XiXi (C) states in female cells and from an Xi state in male cells (D). A scheme (right) and representative simulations (ODE) of Xist levels (left) are shown. (E) 1000 parameter sets were tested for each model. The percentage of sets where the XaXi state is stable (1) and the XiXi state is unstable (2) and the Xi state in male cells is unstable (3) are shown.

Figure 2   *Mutzel et al.*

Figure 2: Mutual repression of Xist and Tsix can maintain the XaXi state

(A-B) Schematic representation of the mathematical model (A) and the simulation (B) shown in C-G to test whether mutual repression of Xist (green) and Tsix (blue) can maintain the Xi state (Xist transcribed, Tsix silenced) on one chromosome and the Xa state (Xist repressed, Tsix transcribed) on the other chromosome in the presence of a single XXA dose. (C) Stochastic simulation of Xist expression in one cell from the two chromosomes (light and dark green) for two example parameter sets. (D) Percentage of parameter sets that maintain the XaXi state in >99% cells for the network shown in (A) and several reduced versions with only one or two repressive mechanisms. (E) The percentage of parameter sets that maintain the XaXi state (black) and that transition to an XiXi state (grey) for different kX-to-kT ratios. (F) For an example parameter set (k_T=113 h^{-1}, $t_{1/2}^{repr}$ =0.7 h) mean and standard deviation of Xist expression from the chromosomes that initiated as Xa (light green) and Xi (dark green), respectively, is shown for different values of k_X. The dotted line indicates the k_X threshold value, above which the Xa state becomes unstable (<99% stable) (G) The distribution of the k_X/k_T ratio at the activation threshold in F for all parameter sets.

Figure 3   *Mutzel et al.*


Figure 3: The model can reproduce mono-allelic Xist up-regulation.

(A+B) Schematic representation of the network and simulation scheme, initiating from the XaXa state in undifferentiated cells where Xist is repressed by pluripotency factors (PP) and Tsix (blue) and XXA (orange) are transcribed. (C) Example simulation of Xist up-regulation in one cell: (top) Xist levels expressed from each chromosome (light and dark green) and (bottom) number of Pol II transcribing Xist (green) and Tsix (blue) or both (black) in a 10-minute time window at the chromosome that up-regulates Xist. (D) The percentage of parameter sets that initiated mono-allelic Xist up-regulation as in (C) in >99% cells for the full model and 2 reduced models (cp. Fig. 2A+D). (E) Schematic diagram of the stability of Xa and Xi (see Fig. 2G) as a function of k_X indicating how k_X is modulated by pluripotency factors (grey, repression) and XXA (orange, activation). (F-I) Analysis of the simulation performed for the reduced model without Xist repression. (F) Distribution of the k_X-to-k_T ratio within all parameter sets that maintain the XaXi state (black) and within the subset that allow mono-allelic Xist up-regulation (grey). (G) Heatmap showing the percentage of parameter sets that allow mono-allelic Xist up-regulation for different combinations of the silencing delays of Tsix and XXA. (H) Example simulations of Xist levels (top) and the Tsix and XXA promoter states (middle) for each X-chromosome (light vs dark colors) in single cells. (bottom) Schematic representation of how k_X (X-axis) and Xist levels (Y axis) change along different routes to the XaXi state due to (1) differentiation, (2) Xist up-regulation, mono-allelic (3a) or bi-allelic (3b) XXA silencing and (4) switch-OFF before silencing in presence of a single XXA dose. (I) The maximal fraction of cells with bi-allelic Xist expression observed during the simulation as a function of the the ratio of switch-ON time (first time point, when >10 Xist molecules have been produced) and XXA silencing delay. Three example simulations are shown.
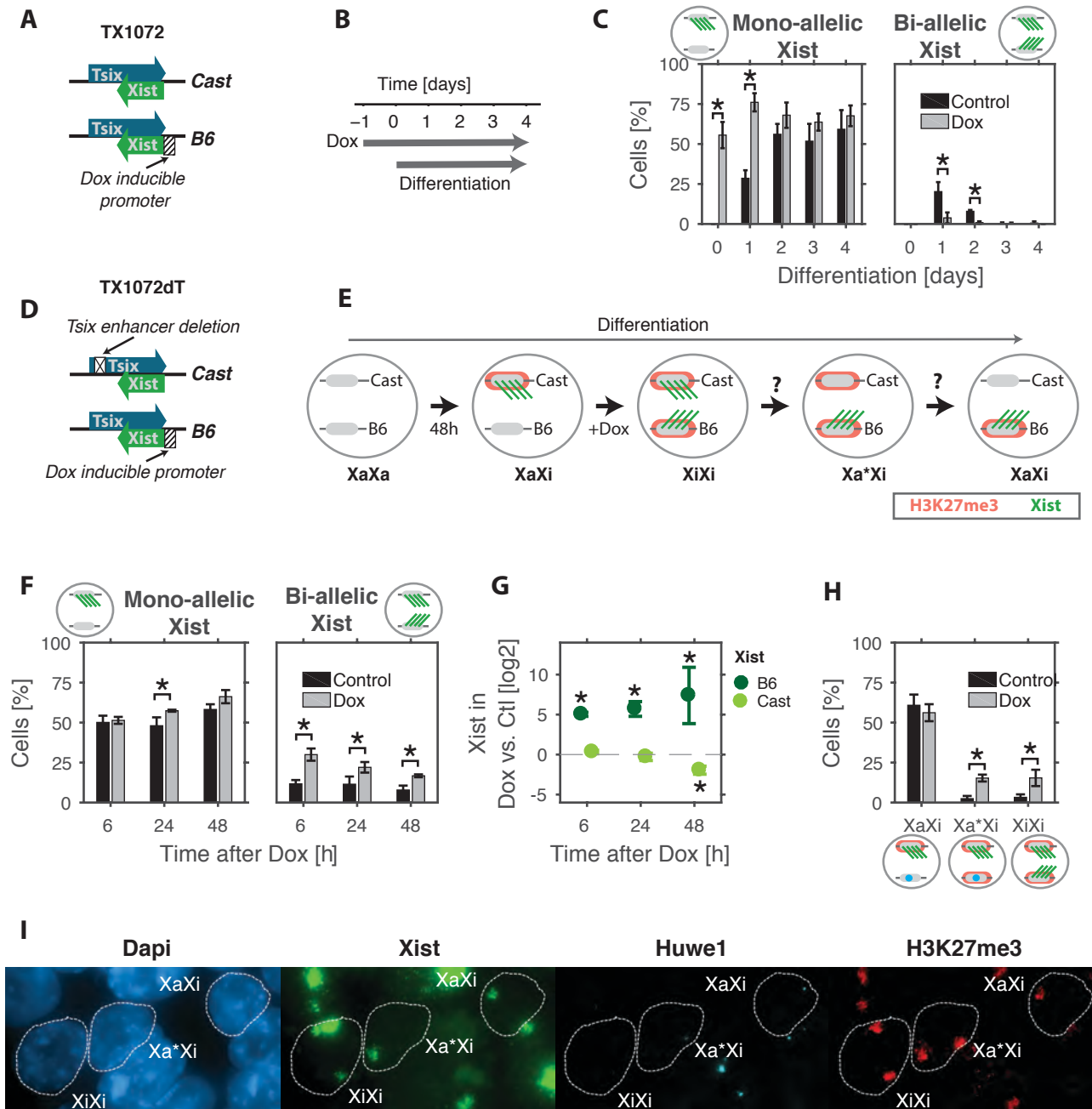
Figure 4

Mutzel et al.
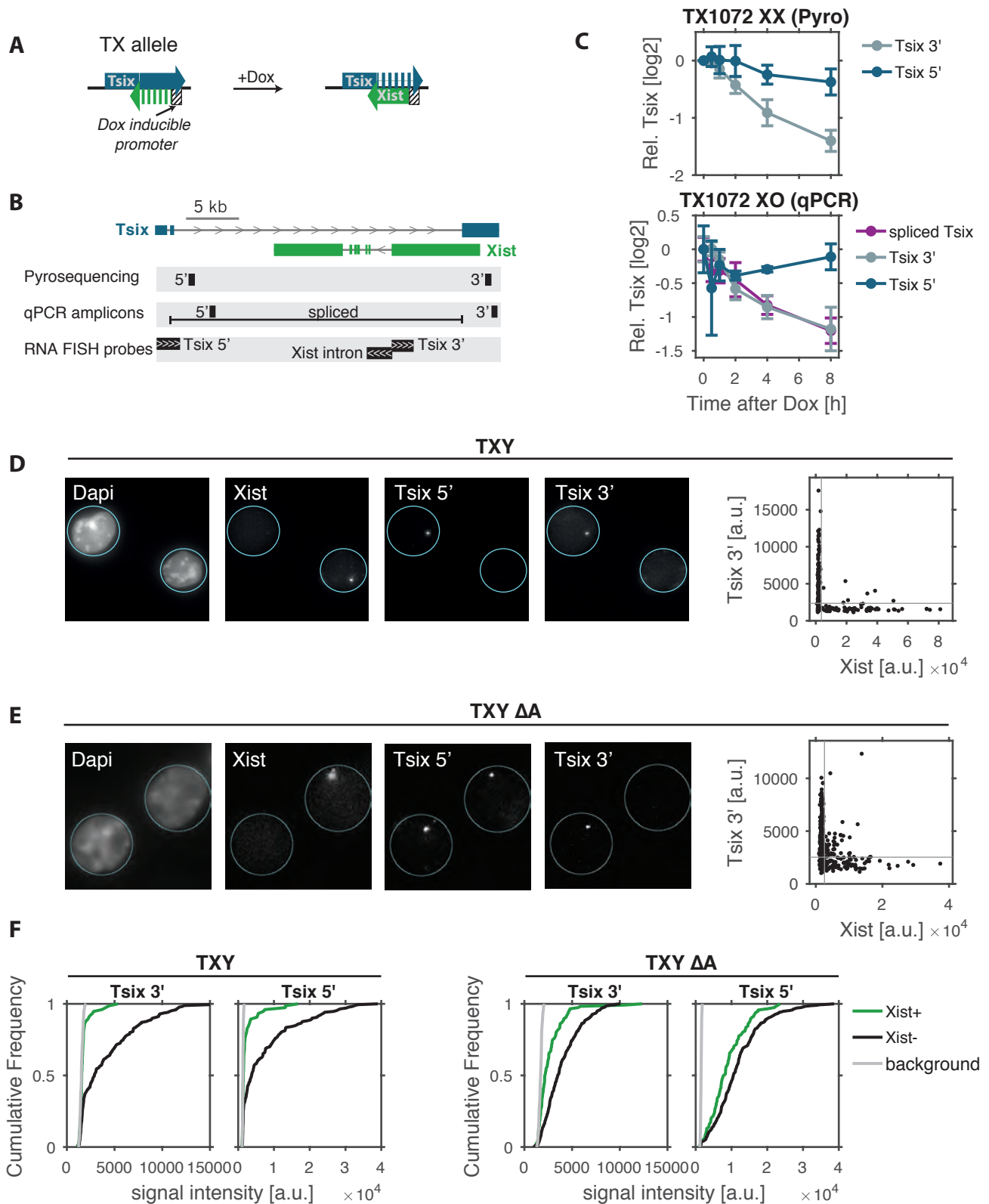
Figure 4: Xist interferes with Tsix elongation

(A) The TX allele carries a Doxycycline inducible promoter driving the endogenous *Xist* gene and was used to investigate whether Xist transcription would interfere with Tsix elongation in (C-F). (B) Position of primers and probes used in (C-F). (C) TX 1072 XX (top) and TX 1072 XO ESCs (bottom) were treated with docycyline for 8 h and Tsix transcription from the TX allele was assessed by pyrosequencing (XX) or qPCR (XO) at different position within the Tsix gene. Mean and standard deviation of three independent experiments is shown. (D-E) TXY (D) and TXY ΔA (E) ESCs were treated with Doxycycline for 24 hours and nascent transcription of Xist and Tsix (5' and 3') was assessed by RNA FISH (probe positions in B). Example images and quantification (right) of 245 (D) and 422 cells (E) is shown. Grey lines indicate the detection threshold estimated from negative control regions. (F) Cumulative distribution of Tsix signal intensity at Xist+ (green) and Xist- alleles (black) in TXY (left) and TXYΔA (right). For (D-F) one out of two experiments is shown.

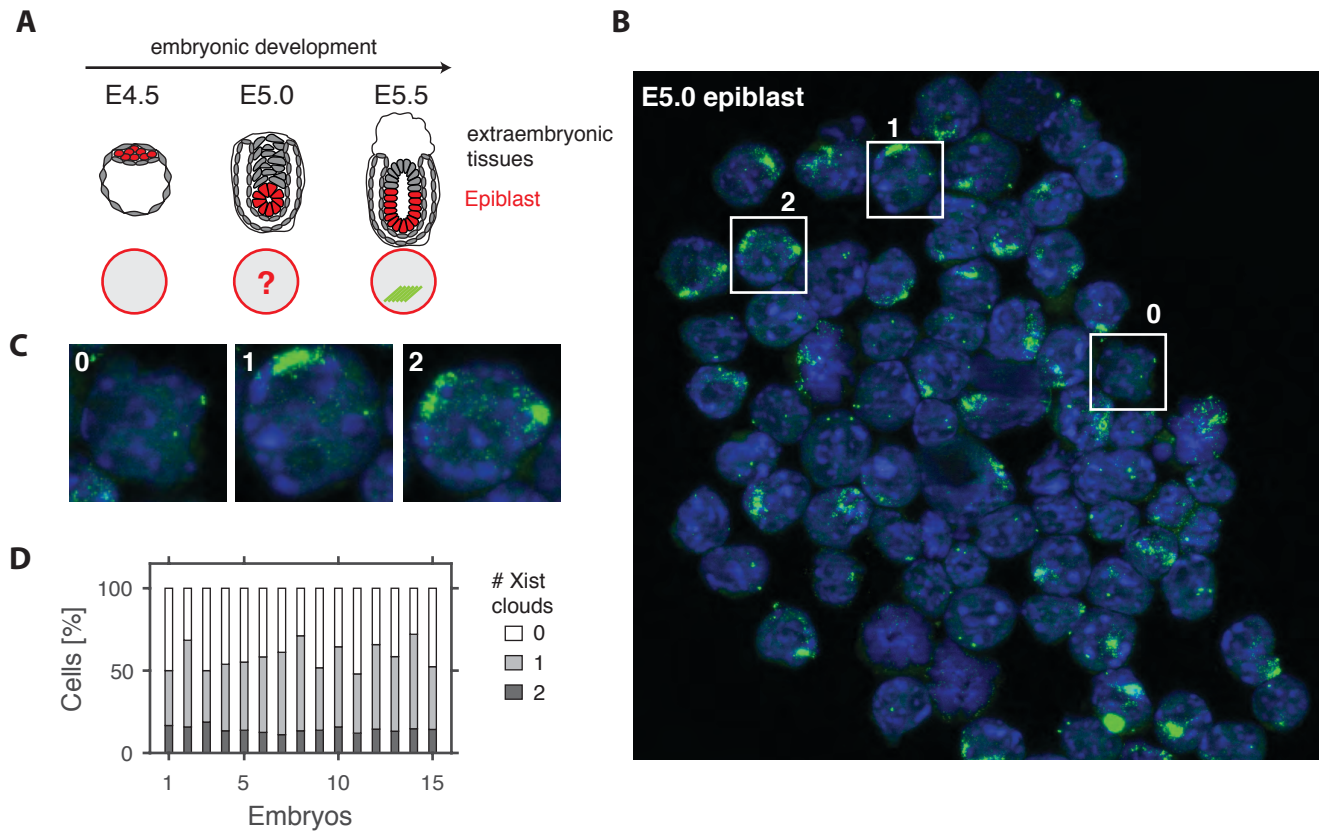**Figure 5**   Mutzel et al.

Figure 5: Bi-allelic Xist up-regulation can be resolved

(A-C) Premature Xist up-regulation by Doxycycline treatment of TX1072 cells (A) one day before differentiation (B). Cells expressing Xist from one (left) or two chromosomes (right) were quantified by RNA-FISH (n>80). (D-I) Bi-allelic Xist up-regulation is artificially induced by treating TXdT1C6 cells (D) with Doxycycline after 48h of differentiation. (E) The model predicts Xist down-regulation from the Cast chromosome, potentially transitioning through an Xa* state, where H3K27me3 (red) is still enriched, while Xist (green) has already been down-regulated. (F) The Xist expression pattern at different time points after Dox addition as assessed by RNA FISH (n>100). (G) Allele-specific analysis of Xist expression by Illumina targeted expression assay at different time points after Dox treatment. (H-I) Immunofluorescence followed by RNA-FISH to detect Xist, H3K27me3 and the nascent transcript of the X-linked gene Huwe1 48h after Dox induction (n>120). Three states were quantified (XaXi, Xa*Xi, XiXi) as shown in the example image (I). Mean and standard deviation of 3 independent experiments are shown. *p<0.05 in two-sample paired (C,F) or one-sample (G) T-test
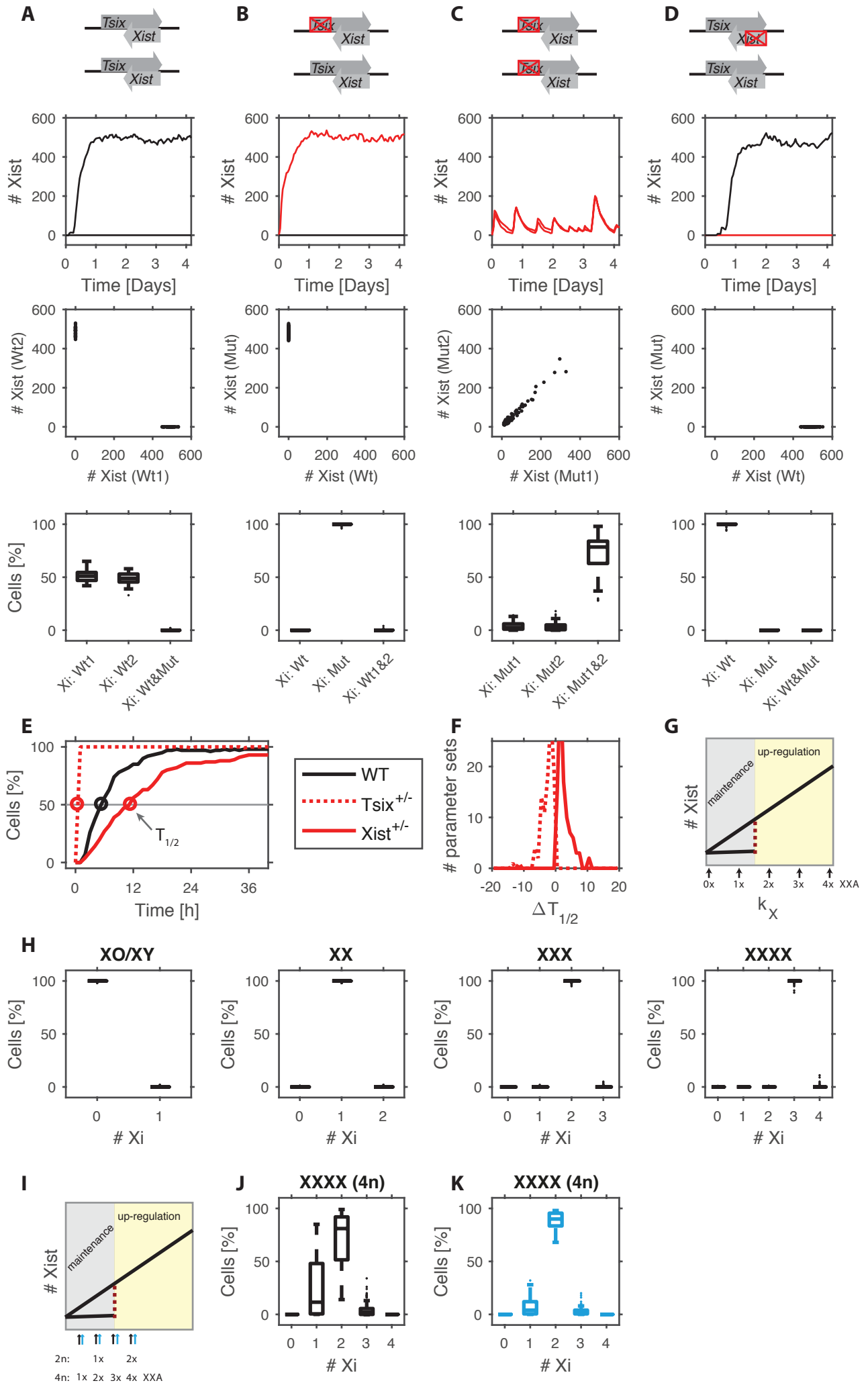
Figure 6

Figure 6: Bi-allelic Xist expression in E5.0 embryos.
(A) Mono-allelic Xist up-regulation occurs between E4.5 and E5.5 of mouse development. (B-C) Xist/Tsix RNA FISH (green) and Dapi staining (blue) of female epiblast cells at E5.0 of embryogenesis. Example cells with 0,1 and 2 Xist clouds are marked and enlarged in (C). (D) Quantification of the number of cells in the epiblast with 0, 1 or 2 Xist-coated chromosomes for 15 female embryos.
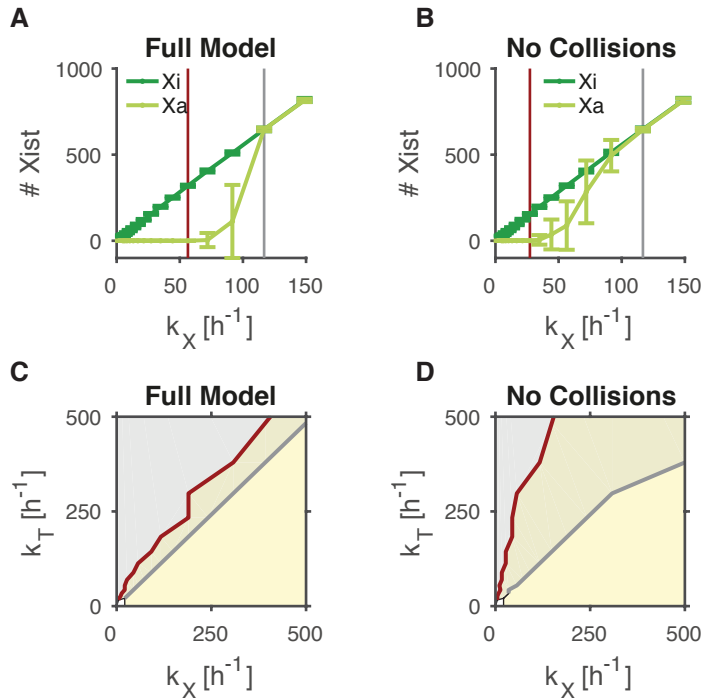
Figure 7   *Mutzel et al.*

Figure 7: Xist/Tsix mutants and X-aneuploidies

(A-D) Simulations of *Xist/Tsix* mutant cell lines (top). Representative simulation of Xist levels produced by the wildtype (black) and mutant (red) chromosomes of a single cell (upper middle) and by 100 cells (lower middle). Boxplot showing the percentage of cells expressing Xist mono-allelically from wildtype or mutant X or bi-allelically for all simulated parameter sets (bottom). (E-F) Xist up-regulation is accelerated in Tsix^{+/-} and delayed in Xist^{+/-} cells. Representative simulation (E) and the distribution of the change of half time ($\Delta T1/2$) in the mutant genotypes (F). (G) Schematic diagram of the stability of Xa and Xi as a function of k_x indicating how different doses of XXA modulate k_x. (H) The percentage of cells with different Xi patterns for 100 parameter sets after 4 days of simulation for cells with 1,2,3 or 4 X-chromosomes. (I) Schematic diagram of the stability of Xa and Xi as a function of k_x indicating how different doses of XXA in diploid (2n) and tetraploid (4n) cells modulate k_x, assuming that a doubling of the nuclear volume in tetraploid cells will result in a two-fold XXA dilution. (J+K) The percentage of cells with different Xi patterns after 4 days of simulation of tetraploid cells for all parameter sets (J) or for those sets (blue in I), where a triple XXA dose resides in the upregulation regime (K).

Supplemental Figure S1   *Mutzel et al.*

Figure S1

(A-D) The simulations carried out to investigate under which conditions the full model and the reduced model without polymerase collisions could maintain the mono-allelic state were compared (see main Fig. 2 and supplemental material). (A+B) For an example parameter set (kT=113 h-1, t_(1/2)^repr =0.7 h) mean and standard deviation of Xist expression from the chromosomes that initiated as Xa (light green) and Xi (dark green), respectively, is shown for different values of kx for the full model (A) and the reduced model without collisions (B). The vertical lines indicate the kX threshold value, above which >1 (red) or >99 (grey) out of 100 cells up-regulate Xist from the Xa. (C+D) The parameter regimes where the XaXi state is maintained (grey) or Xist is up-regulated from the Xa (yellow) in >99 out of 100 cells are show in the kX/kT space for the Full model (C) and the reduced model without collisions (D). Red and grey lines indicate the activation threshold as in (A+B).

1 Experimental Procedures

1.1 Mice

All experimental designs and procedures were in agreement with the guidelines from French and Japan legislations and institutional policies. Embryos were obtained by natural mating between B6D2F1 (derived from C57BL/6J and DBA2 crosses) female and males. Noon of the day when vaginal plugs were detected was set as E0.5.

1.2 Cell lines

The female TX1072 cell line and its subclone TX1072 XO (clone A11) are F1 hybrid ESCs (CastxB6) that carry a doxycycline responsive promoter in front of the *Xist* gene on the B6 chromosome and an rtTA insertion in the Rosa26 locus (described in (Schulz et al., 2014)). The TXdT line (clone 1C6) was generated by introducing a deletion of the Dxpas34 repeat in TX1072 cells on the Cast chromosome by co-transfecting Cas9 expression vectors p330 expressing sgRNAs GTACATAATGACCCGATCTC and GAACTCACTATATCGCCAAAG (Ran et al., 2013). Clones with the deletion were identified by PCR (ES585:AGGCACACCACCCCAGTGGA, ES609:TCCAAACATGGCGGCAGAAGC) and the deleted allele was identified by Sanger sequencing of the PCR product using primer ES609 based on two SNPs at positions 100,645,601 (Cast: C) and 100,641,221 (Cast: G) (mm9). Male-inducible wild-type and ΔA *Xist* lines were a gift from A. Wutz (called Xist-tetOP and Xist-ΔSX-tetOP, respectively, in (Wutz et al., 2002))

1.3 ES cell culture and differentiation

TX1072, TX1072 XO and TXdTC6 cells were grown on gelatin-coated flasks in serum-containing ES cell medium (DMEM (Sigma), 15% FBS (Gibco), 0.1mM β-mercaptoethanol, 1000 U/ml leukemia inhibitory factor (LIF, Chemicon)), supplemented with 2i (3 µM Gsk3 inhibitor CT-99021, 1 µM MEK inhibitor PD0325901) for TX1072 and TX1072 XO. Differentiation was induced by 2i/LIF withdrawal in DMEM supplemented with 10% FBS and 0.1mM β-mercaptoethanol at a density of $4*10^4$cells/cm^2 in Fibronectin (10 µg/ml) coated tissue culture plates. For ectopic *Xist* induction the medium was supplemented with 1 µg/ml Doxycycline. To induce *Xist* in undifferentiated cells, they were plated at a density of $1*10^5$cells/cm^2 two days before the experiment and then treated with 1 µg/ml Doxycycline. Male-inducible wild-type and ΔA *Xist* lines were grown on mitomycin-C-inactivated mouse embryonic fibroblasts in ES cell media containing 15% FBS (Gibco), 0.1mM β-mercaptoethanol (Sigma), 1,000 U/ml LIF (Chemicon) and treated for 24 h with 2 µg/ml doxycycline.

1.4   Conventional RNA FISH on ESCs

FISH on cells from tissue culture was performed as described previously (Chaumeil et al., 2008). Briefly, mESCs were dissociated using Accutase (Invitrogen) and adsorbed onto Poly-L-Lysine (Sigma) coated coverslips #1.5 (1mm) for 5 min. Cells were fixed with 3% paraformaldehyde in PBS for 10 min at room temperature and permeabilized for 5 min on ice in PBS containing 0.5%Triton X-100 and 2mM Vanadyl-ribonucleoside complex (New England Biolabs). Coverslips were preserved in 70% EtOH at -20°C. Prior to FISH, samples were dehydrated through an ethanol series (80%, 95%,100% twice) and air-dried quickly. For detecting Huwe1, a BAC spanning the respective genomic region (RP24-157H12) was labeled by nick translation (Abbot) using dUTP-Atto550 (Jena Bioscience). Per coverslip, 60ng probe was ethanol precipitated with Cot1 repeats, resuspended in formamide, denatured (10min 75ºC) and competed for 1h at 37ºC. *Xist* was detected with a custom designed strand-specific probe that covers all exons with ~75bp long oligo nucleotides end-labeled with the Alexa488 fluorophore (Roche). Both probes were co-hybridized in FISH hybrization buffer (50% Formamide, 20% Dextran sulfate, 2x SSC, 1µg/µl BSA, 10mM Vanadyl-ribonucleoside) over night. Washes were carried out at 42°C three times 7min in 50% formamide in 2X SSC at pH=7.2 and three times 5min in 2X SSC. 0.2mg/mL DAPI was used for counterstaining and mounting medium consisted in 90% glycerol, 0.1X PBS, 0.1% p-phenylenediamine at pH9 (Sigma). Images were acquired using a wide-field DeltaVision Core microscope (Applied Precision) or a widefield Z1 Observer (Zeiss) using a 100x objective.

1.5   Immunofluorescence combined with RNA FISH

For immunofluorescence staining cells were differentiated on Fibronectin coated cover slips (18mm Marienfeld) at a density of $2*10^4$cells/cm^2. Cells were fixed and permeabilized as described above and incubated with the H3K27me3 antibody (Active Motif #39155, 0.4ug/ml) in PBS for 1h at room temperature, then washed 3 times for 10 minutes with PBS, followed by a 1h incubation with an Alexa-555 labelled Goat anti-rabbit antibody (Invitrogen A-21428, 0.8 ug/ml). After 3 washes, the cells were fixed again with 3% paraformaldehyde in PBS for 10 min at room temperature, followed by three short washes with PBS and two washes with SSC. Hybridization was then performed as described in 1.4.

1.6   Quantitative RNA FISH

Quantitative RNA FISH on *Xist* and *Tsix* was performed using Stellaris FISH probes (Biosearch Technologies). Cells were adsorbed and fixed as described above. Cells were prehybridized in wash buffer (2x SSC, 10% formamide) twice for 5 min, then hybridized with a solution that contained 125 nM of each FISH probe, 2X SSC, 10% formamide, 10%

dextran sulfate overnight at 37 °C. Cells were washed twice with wash buffer for 30 min before counterstaining DNA with 0.2mg/ml DAPI in 1x PBS, and mounted on slides using the mounting medium described above. Z-stacks were acquired using a wide-field DeltaVision Core microscope microscope equipped with a 100x objective (voxel size 129x129x200 nm). Quantification of nascent RNA signals was performed as in (Giorgetti et al., 2014). Briefly, the fluorescence background of each z plane was generated by morphologically opening the image with a circular structuring element with a diameter of 5 pixels (645 nm), and subtracted from the original image. A region of interest (ROI) of constant volume (30x30x6 pixels = 1.3x1.3x1.2μm) was selected around each transcription site. To reduce residual high-frequency fluorescence background, the average pixel intensity was measured in a 3-voxel thick frame adjacent to the border of the ROI, and further subtracted. The integrated intensity of the fluorescent signal was then measured within the whole ROI. Integrated intensities of approximately 200 random nuclear background ROIs were used to define a threshold to classify transcribed versus non transcribed loci.

1.7 RNA FISH of epiblast cells from E5.0 embryos

For E5.0 mouse embryos, the embryos were dissected out from decidua and the Reichert's membrane was removed in a 6cm Petri dish containing PBS using sharpened forceps. Extra embryonic ectoderm was separated by a fine glass needle. The epiblast/visceral endoderm were incubated in 0.25% Pancreatin (Sigma) / 0.5% Trypsin / Polyvinylpyrrolidone (PVP40; Sigma) at 4°C for 10min and transferred to a 3.5cm petri dish containing a large volume of 1%BSA/PBS. Epiblast and visceral endoderm were separated by pipetting with a mouth pipette whose internal diameter is slightly smaller than that of epiblast. RNA FISH were carried out as described previously (Okamoto et al., 2004), using a non strand-specific probe detecting *Xist* and *Tsix*. Embryos with an *Xist* cloud were identified as female. Images were acquired using a 200M Axiovert fluorescence microscope (Zeiss) equipped with an ApoTome was used to generate 3D optical sections. Sequential z-axis images were collected in 0.3 μ m steps. Images were analyzed using ImageJ software (Fiji, NIH).

1.8 RNA extraction, reverse transcription, qPCR

For pyrosequencing and qPCR, cells were lysed by direct addition of 1 ml Trizol (Invitrogen). Then 200μl of Chloroform was added and after 15 min centrifugation (12000xg, 4°C) the aqueous phase was mixed with 700 μl 70% ethanol and applied to a Silica column (Qiagen RNAeasy Mini kit). RNA was then purified according to the manufacturer's recommendations, including on-column DNAse digestion. For quantitative PCR (qPCR), 1ug RNA was reverse transcribed using Superscript III Reverse

Transcriptase (Invitrogen). Expression levels were quantified using 2x SybRGreen Master Mix (Applied Biosystems) and a ViiA7 system (Applied biosystems) with ~8ng cDNA and the primers given in Table S1. Expression levels were normalized to Rrm2 and Rplp0.

1.9   Targeted RNA Expression Assay

For allele-specific quantification of *Xist* expression the TruSeq Targeted RNA Expression assay (Illumina) was used according to the manufacturer's recommendations. RNA was extracted using the Direct-zol RNA MiniPrep kit (Zymo Research) and DNase digest was performed using Turbo DNA free kit (Ambion). Four amplicons containing SNPs within *Xist* were measured and normalized to amplicons in four autosomal reference genes (Rrm2, Rplp0, Fbxo28, Exoc1). Details on the amplicons are given in supplementary table S1. Read counts of each *Xist* amplicon mapping to the B6 and Cast alleles, respectively, were normalized to the geometric mean of the four reference genes. The fold change of the doxycycline treated sample relative to the corresponding control sample was then calculated for each *Xist* amplicon. Using a one-sample t-Test it was tested whether the mean log2 fold-change of the four amplicons was significantly different from 0 ($p<0.05$).
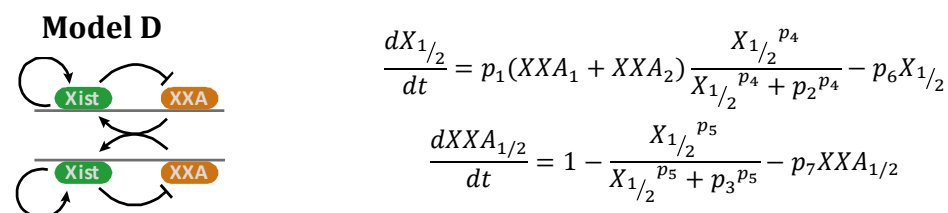
1.10 Pyrosequencing

For allele-specific expression analysis of *Tsix*, pyrosequencing technology was used. Two different amplicons within *Tsix*, each containing a SNP were PCR-amplified from cDNA with biotinylated primers and sequenced using the Pyromark Q24 system (Qiagen). Primer sequences are given in supplemental Table S1. The assay provides the fraction of *Tsix* transcript arising from the B6 chromosome at time t (F_t). To calculate the expression from the B6 chromosome at time t relative to the uninduced state at t=0h ($\frac{B6_t}{B6_0}$) the data was transformed as follows. Assuming that expression from the Castaneus chromosome (Cast) is constant over time, $F_0 = \frac{B6_0}{B6_0+Cast}$ and $F_t = \frac{B6_t}{B6_t+Cast}$ can be transformed into $\frac{B6_t}{B6_0} = \frac{F_t(1-F_0)}{F_0(1-F_t)}$

2   Computational Methods

2.1   Deterministic Model

2.1.1   Role of positive and negative feedback

To investigate which network modules are required for stable mono-allelic expression, the four different networks shown below were simulated as ordinary differential equations. Each model has four variables (2 copies of *Xist* (=X), 2 copies of XXA).

Model A

$$\frac{dX_{1/2}}{dt} = p_1(XXA_1 + XXA_2) - p_6 X_{1/2}$$

$$\frac{dXXA_{1/2}}{dt} = 1 - p_7 XXA_{1/2}$$

Model B

$$\frac{dX_{1/2}}{dt} = p_1(XXA_1 + XXA_2) - p_6 X_{1/2}$$

$$\frac{dXXA_{1/2}}{dt} = 1 - \frac{X_{1/2}^{p_5}}{X_{1/2}^{p_5} + p_3^{p_5}} - p_7 XXA_{1/2}$$

Model C

$$\frac{dX_{1/2}}{dt} = p_1(XXA_1 + XXA_2)\frac{X_{1/2}^{p_4}}{X_{1/2}^{p_4} + p_2^{p_4}} - p_6 X_{1/2}$$

$$\frac{dXXA_{1/2}}{dt} = 1 - p_7 XXA_{1/2}$$

Model D

$$\frac{dX_{1/2}}{dt} = p_1(XXA_1 + XXA_2)\frac{X_{1/2}^{p_4}}{X_{1/2}^{p_4} + p_2^{p_4}} - p_6 X_{1/2}$$

$$\frac{dXXA_{1/2}}{dt} = 1 - \frac{X_{1/2}^{p_5}}{X_{1/2}^{p_5} + p_3^{p_5}} - p_7 XXA_{1/2}$$
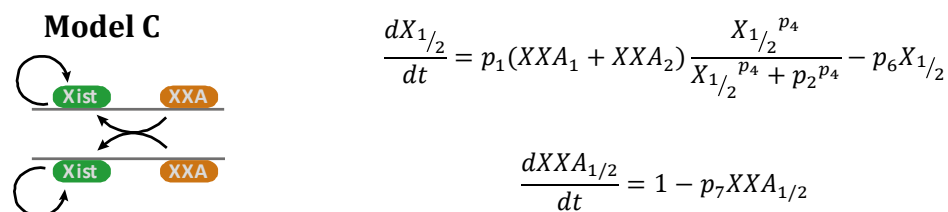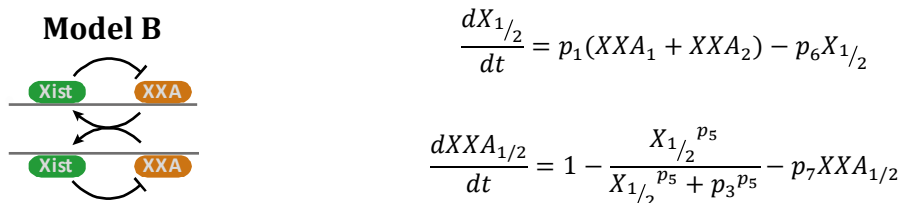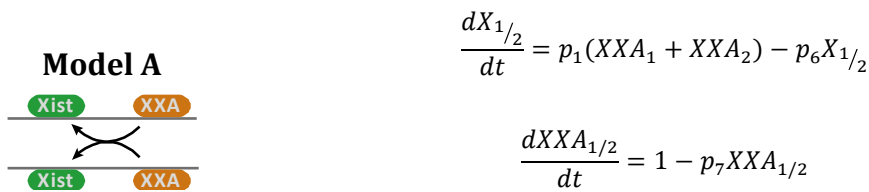
The most complex network contains 7 different parameters. Two of these, the *Xist* and XXA degradation rates, were kept constant. For the *Xist* half-life previous studies have attempted an experimental estimation, resulting in values of 2 and 6h respectively (Sun et al., 2006; Yamada et al., 2015). We therefore use the mean (4h), which results in a degradation rate of 0.1733 h^{-1} (ln(2)/t$_{1/2}$). For simplicity, the degradation rate of XXA was set to 1 h^{-1}. For hill coefficients, values of 1,2 and 10 were tested and for all other

parameters a series of randomly chosen values within a realistic parameter range (given in the table below) were used.

Description	Parameter	Parameter value(s)
Xist transcription rate [h^{-1}]	p$_1$	10-1000 (log distributed)
Threshold (pos. FB) [# mol]	p$_2$	10-1000 (log distributed)
Threshold (XA silencing) [# mol]	p$_3$	10-1000 (log distributed)
Hill coef. (pos FB)	p$_4$	1, 2, 10
Hill coef. (XA silencing)	p$_5$	1, 2, 10
Xist degradation [h^{-1}]	p$_6$	0.1733
XXA degradation [h^{-1}]	p$_7$	1

2.1.2 Is mono-allelic expression stable?

To assess which network can maintain stable mono-allelic expression, cells with one active X (Xa), where *Xist* expression is low and with one inactive X (Xi), where *Xist* expression is high were simulated. The initial condition of *Xist* on the Xi was set to 2p$_1$/p$_4$, which gives the maximal *Xist* level in the presence of two XXA doses and XXA was set to 0. On the Xa the initial condition for *Xist* was set to 1 and XXA was set to 1. To reach the steady state each simulation was carried out for 10,000 h using the ode15s integrator in Matlab. For each network 1000 randomly chosen parameter sets were simulated. Based on the steady state reached at the end of the simulation, a parameter set was classified as mono-allelic, if the following conditions were met: *Xist* on Xa<0.1 & *Xist* on Xi>0.1. As shown in the table below only networks containing a positive feedback loop can maintain mono-allelic expression (XaXi stable).

# parameter sets	Model A	Model B	Model C	Model D
total	1000	1000	1000	1000
XaXi stable	0	0	466	423
XaXi stable & XiXi unstable			0	101
XaXi stable& XiXi unstable & Xi unstable				101

2.1.3   Is bi-allelic expression unstable?

For each mono-allelic parameter set, a second simulation was performed to determine, whether a bi-allelic state (XiXi) would also be stable. In this case the initial conditions for *Xist* were set close to the maximal value on both chromosomes with $2*q*p_1/p_4$ with q being a random number between 1.0 and 1.1, and the initial level of XXA was set to 0. Based on the steady state reached in the simulation, those parameter sets, where the bi-allelic state was unstable were identified as those sets, where *Xist* on at least one of the two chromosomes was <0.1. As shown in the table above only for the network which contains a negative feedback in addition to the positive feedback loop, parameter sets are found, where bi-allelic expression was unstable (XaXi stable & XiXi unstable).

2.1.4   Is *Xist* expression maintained in male cells?

For each mono-allelic parameter set, where bi-allelic expression was unstable, another simulation was performed to determine, whether *Xist* expression from the single X chromosome in male cells would be stable. Here the network only contained two variables, one copy of *Xist* and one copy of XXA. The initial conditions for *Xist* were set to the maximal value p_1/p_4, and the levels for XXA were set to 0. Based on the steady state reached in the simulation, those parameter sets, where expression was not maintained were identified as those sets, where *Xist* expression was <0.1. As shown in the table above, for all mono-allelic parameter sets, where biallelic expression was unstable, also expression in male cells was not maintained.

2.1.5   Parameter rules

To understand the prerequisites for stable mono-allelic expression, we first assessed which interactions in Model D required cooperativity. The parameter sets tested were divided in four groups, according whether cooperativity is assumed for the positive feedback loop ($p_4>1$) and/or for XXA silencing ($p_5>1$). As shown in the table below, only cooperativity in the positive feedback loop was required for stable mono-allelic expression.

# parameter sets	p4=1 p5=1	p4>1 p5=1	p4=1 p5>1	p4>1 p5>1
total	111	215	237	437
XaXi stable	0	139	0	284
XaXi stable & XiXi unstable	0	28	0	73
XaXi stable & XiXi unstable & Xi unstable	0	28	0	73

Furthermore, the *Xist* level reached with maximal transcription rate, given by p_1/p_6 must be higher than the threshold for the positive feedback p_2. This can be seen in the following plots, where mono-allelic parameter sets are colored in red.
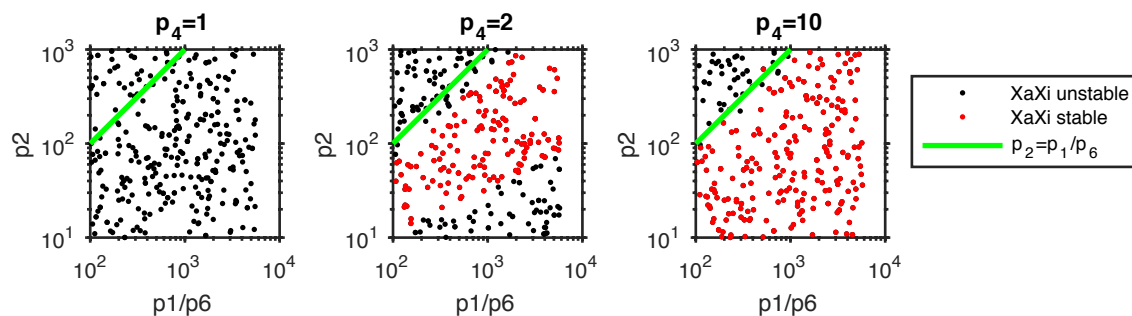
Finally, we analyzed the parameter sets that allowed mono-allelic expression with respect to their ability to maintain bi-allelic expression. Only if the threshold for XXA silencing (p_3) lies at least in the same range as the threshold of the positive feedback p_2, bi-allelic expression will be unstable (green in the plot below). Only if this condition is met, XXA will be efficiently silenced, making the negative feedback functional.
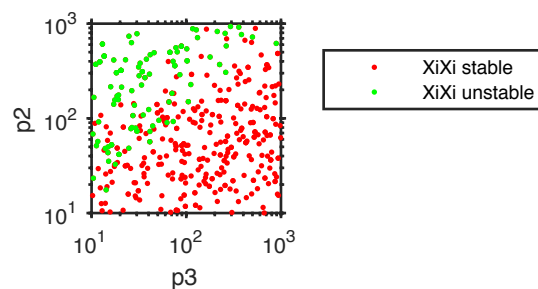
2.2 Stochastic Simulations of XaXi maintenance

2.2.1 Model Reactions

To test the maintenance of the XaXi state (Fig. 2, main text), reactions describing transcription initiation, transcription elongation and RNA degradation of *Xist* and *Tsix* were combined into a mathematical model (see scheme below).
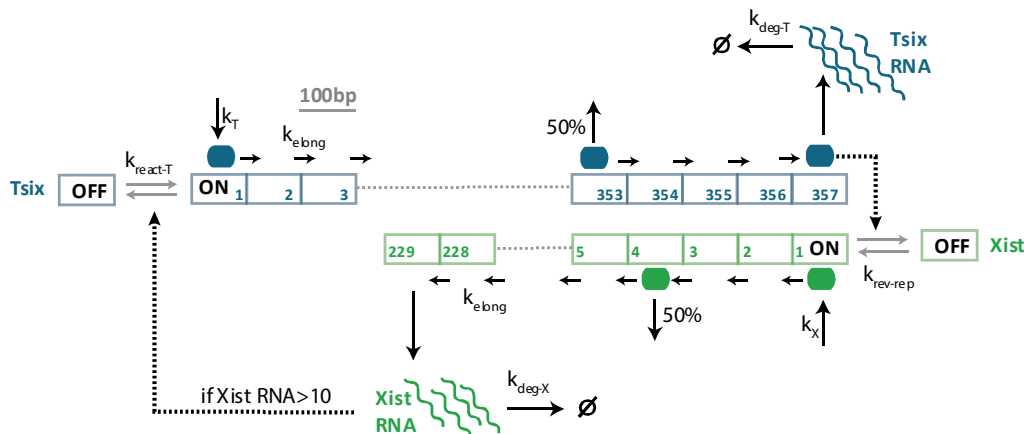
Both promoters were assumed to exist in an 'OFF' state, where no transcription occurs, and an 'ON' state, where transcription is initiated with constant transcription rates k_X and k_T. The *Tsix* promoter is turned off by *Xist* RNA-mediated silencing, the *Xist* promoter is turned off by passing *Tsix* polymerases. The OFF state is reverted back to the ON state with rate $k_{rev-rep}$. To describe transcriptional elongation, the *Xist* and *Tsix* gene bodies were divided into segments of 100nt and polymerases move along the gene body with a constant rate (k_{elong}). Fully elongated transcripts produce one RNA molecule. Degradation of the RNA obeys first-order reaction kinetics with the rates k_{deg-X} and k_{deg-T}.

Transcription of *Xist* and *Tsix* mutually interfere by the following mechanisms: (i) RNA Pol II collisions occur between sense- and antisense transcribing polymerases with one randomly chosen polymerase being removed from the gene; (ii) *Tsix* polymerases transcribing through the *Xist* promoter region induce a transition to the OFF state of the *Xist* promoter that can be reverted to the ON state with $k_{rev-rep}$ (the half live the repressed state is given by $t_{1/2}^{repr} = \frac{ln2}{k_{rev-rep}}$); (iii) Silencing of the *Tsix* promoter by *Xist* RNA: If *Xist* RNA is present above a threshold level of 10 RNA molecules it induces a transition of the *Tsix* promoter to the OFF state. Since the maintenance model was only used to simulate the steady state in cells where XCI has already occurred, silencing is assumed to be already established at the beginning of the simulation (see Xi initial condition below in 2.2.3). Therefore the kinetics of silencing do not affect the outcome of the simulation and are thus described in detail only below for the model of monoallelic

Xist upregulation (2.3). Similarly, the XXA is present at a constant single dose in post-XCI cells with a single Xa and is therefore not explicitly accounted for in the maintenance model.

2.2.2 Parameter values

Degradation and elongation rates were set to fixed values based on previous experimental estimates. All other parameters were varied within realistic parameter ranges and systematically combined resulting in 8000 parameter sets in total (see following table).

Description	Parameter	Parameter value(s)
Xist transcription rate [h^{-1}]	k_X	5, 6.35, 8.1, 10.35, 13.2, 16.8, 21.4, 27.3, 34.75, 44.3, 56.45, 71.9, 91.65, 116.8, 148.8, 189.65, 241.65, 307.95, 392.4, 500
Tsix transcription rate [h^{-1}]	k_T	as k_X
Xist degradation rate [h^{-1}]	k_{deg-X}	0.1733 (Sun et al., 2006; Yamada et al., 2015)
Tsix degradation rate [h^{-1}]	k_{deg-T}	1.3868 (Sun et al., 2006)
Elongation rate [bp/sec]	k_{elong}	40 (Jonkers et al., 2014)
Reversal rate of *Xist* promoter repression [h^{-1}]	$k_{rev-rep}$	0.1, 0.1438, 0.2069, 0.2976, 0.4281, 0.6159, 0.8859, 1.2743, 1.8330, 2.6367, 3.7927, 5.4556, 7.8476, 11.288, 16.238, 23.357, 33.598, 48.329, 69.519, 100

2.2.3 Initial conditions

To investigate the stability of the Xa and Xi, each state was simulated using the initial conditions given in the table below. The RNA levels for transcribing genes was set to their maximal steady state value and the polymerase complexes were randomly distributed along the gene body.

	Xi	Xa
Xist RNA	k_X/k_{deg-X}	0
Tsix RNA	0	k_T/k_{deg-T}
Xist promoter	ON	OFF
Tsix promoter	OFF	ON
# *Xist* polymerases	$\frac{L}{k_{elong}} * k_X$ (L=22 900 bp)	0
# *Tsix* polymerases	0	$\frac{L}{k_{elong}} * k_T$ (L=35 700 bp)

2.2.4   Simulations

All simulations were conducted in MATLAB. The model was written in C++ and compiled into a MEX file that was called from the main MATLAB function. For parameter scanning a compiled Matlab script was executed in parallel on a computing cluster. In the simulation, transcription elongation occurs at fixed time intervals of 2.5 seconds inferred from measurements of polymerase speed (elongation of one 100bp interval at k_{elong}=40bp/sec). Between elongation steps, all other reactions are simulated using the stochastic Gillespie algorithm (Gillespie, 1977). For each parameter set 100 Xi/Xa pairs were simulated for 500h to reach the steady state.

2.2.5   Simulation analysis

A simulation was classified as stably maintaining the XaXi state if *Xist* was on average present with >10 molecules at the Xi and with <10 molecules at the Xa during the last 50h of the simulation. Parameter sets, where >99% of Xa/Xi pairs were stably maintained (XaXi) as well as those sets where >99% of Xa/Xi pairs transitioned to an XiXi state (XiXi) were identified (Fig. 2C-E). Based on the systematic variation of k_X, two thresholds were determined. For values below the lower activation threshold >99% of Xa/Xi pairs are stable (Fig. 2F, Fig. S1), while above the upper threshold <1% Xa/Xi pairs are stable (Fig. S1).

2.2.6   Reduced models

To analyze which of the repressive mechanisms are strictly required for stable maintenance of the Xa/Xi state, we systematically investigated all possible combinations of reduced model structures with all three, a combination of two or only a single repressive mechanism (Fig. 2D, main text).

- In all models without *Xist* promoter repression, passing *Tsix* polymerases do not affect the *Xist* promoter state (parameter $k_{rev-rep}$ removed).
- In all models without *Tsix* promoter silencing, the *Xist* RNA does not affect the *Tsix* promoter state.
- In all models without polymerase collisions, *Xist* and *Tsix* polymerases were assumed to be able to bypass each other.

The reduced models were simulated and analyzed as described above with the parameters values for k_X, k_T and $k_{rev-rep}$ (where applicable) given in 2.2.2. As shown in the following table *Xist* RNA-mediated silencing of *Tsix* and at least one additional mechanism are required to maintain the XaXi state stably in >99% cells.

Model	parameters varied	# parameter sets tested	XaXi stable [%]
Tsix silencing, *Xist* repression and Polymerase collisions	k_X, k_T, $k_{rev-rep}$	8000	50%
Xist repression and Polymerase collisions	k_X, k_T, $k_{rev-rep}$	8000	0%
Tsix silencing and Polymerase collisions	k_X, k_T	400	45%
Tsix silencing and *Xist* repression	k_X, k_T, $k_{rev-rep}$	8000	26.4%
Tsix silencing	k_X, k_T	400	0%
Xist repression	k_X, k_T, $k_{rev-rep}$	8000	0%
Polymerase collisions	k_X, k_T	400	0%

2.3 Stochastic simulation of mono-allelic up-regulation

2.3.1 Role of XXA

To simulate a female cell during the onset of XCI, two chromosomes as described in section 2.1. were coupled by a negative feedback mediated by XXA (Fig. 3, main text). The XXA concentration was modeled as a step function with the value 1 if the respective XXA allele is active and the value 0 if the respective XXA allele has been silenced by *Xist* RNA. The kinetics of RNA and protein decay of XXA were not accounted for explicitly but were instead assumed to modulate the XXA silencing kinetics (see below). The XXA dosage modulates the effective *Xist* initiation rate k_X^{eff} as follows:

$$k_X^{eff} = q_{XXA} \cdot k_X$$

where k_X is the *Xist* initiation rate in the presence of a single XXA dose and $q_{XXA}=0,1,2$ depending on whether no, one or two XXA loci are active.

2.3.2 Role of differentiation

To reproduce coupling of XCI to development, k_X^{eff} must be influenced by the differentiation timing, representing the action of stem cell specific factors that prevent *Xist* upregulation in undifferentiated cells by repressing *Xist*. The differentiation dependency was formulated as a step function that changes its value at the point of induction of differentiation such that k_X^{eff} prior to differentiation was one-tenth of the k_X value after the onset of differentiation.

Before differentiation: $\qquad k_X^{eff} = 0.1 \cdot q_{XXA} \cdot k_X$

After onset of differentiation: $\quad k_X^{eff} = q_{XXA} \cdot k_X$

2.3.3 *Xist*-dependent silencing

Since *Xist*-dependent silencing is known to occur with a delay of hours or days after *Xist* has been up-regulated (Chow et al., 2010), we implemented a silencing delay described by the parameters sil_{Tsix} or sil_{XXA}. To this end, each chromosome passes stochastically through a number of intermediate states S1, S2...Sn once *Xist* expression from that chromosome has exceeded a certain threshold (10 molecules) and gene silencing occurs once the final silencing state Sn has been reached. If the level of *Xist* RNA molecules drops below the threshold before Sn has been reached, the chromosome immediately passes back to the unsilenced state S0. The transitions through the intermediate states occur with rate $1h^{-1}$ such that the number of intermediate states given by the model parameters sil_{Tsix} or sil_{XXA} is equal to the mean silencing delay. Silencing is assumed to be reversed, if the *Xist* level drops below the threshold of 10 molecules. Reactivation of *Tsix* and XXA will then occur with a single stochastic reaction with the rates $k_{react-T}$ and $k_{react-XXA}$ respectively (see figure below).

Forward reactions: Xist RNA > 10
Reverse reactions: Xist RNA < 10
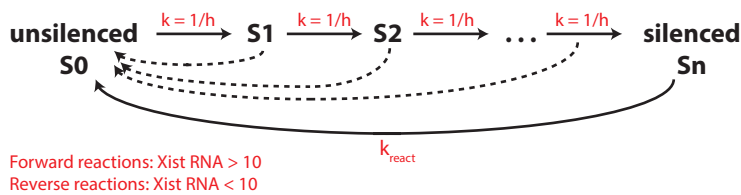
2.3.4 Simulations

To simulate the onset of X-inactivation, both chromosome were initiated from the Xa state (see 2.2.3) in undifferentiated cells with double XXA dosage present (q_{XXA}=2). *Xist* up-regulation was simulated for all model structures and parameter sets that could stably maintain the XaXi state in section 2.2 (Full model: 4001 sets, model with *Tsix* silencing and Polymerase collisions: 180 sets, model with *Tsix* silencing and *Xist* repression: 2115 sets). Each parameter set was combined with 500 combinations of randomly sampled values for sil_{XXA}, sil_{Tsix}, $k_{react-XXA}$ and $k_{react-T}$ (see following table).

Description	Parameter	Parameter values
Silencing delay of XXA [h]	sil_{XXA}	1 – 48 (log distributed)
Silencing delay of *Tsix* [h]	sil_{Tsix}	1 – 48 (log distributed)
Reactivation rate of XXA [h^{-1}]	$k_{react-XXA}$	0.1-100 (log distributed)
Reactivation rate of *Tsix* [h^{-1}]	$k_{react-T}$	0.1-100 (log distributed)

For each parameter set 100 cells were simulated. To reach the steady state prior to differentiation, the cells were simulated for 10h in an undifferentiated state, then 100 hours of differentiation were simulated as this is the relevant time scale of XCI. Each cell was classified as monoallelic, if during the last 20h of the simulation >10 molecules of *Xist* RNA were present on average at one chromosome (Xi) and <10 molecules on the other (Xa). A parameter set was classified as monoallelic if >99% of cells upregulated *Xist* monoallelically (XaXa->XaXi in Fig. 3D-G in the main text). The following table summarizes how many of the parameter sets exhibited mono-allelic (MA) up-regulation for each of the model structures revealing that polymerase collisions are required for MA up-regulation of *Xist*.

| Model	Parameter Sets tested	Monoallelic sets
Tsix silencing, *Xist* repression and Polymerase collisions	2 000 500	1.17 % MA in >99% of cells
Tsix silencing and Polymerase collisions	90 000	1.53 % MA in >99% of cells
Tsix silencing and *Xist* repression	1 057 500	0 % MA in >99% of cells

To keep the model as simple as possible, all further analyses were conducted using the reduced model without *Xist* repression.

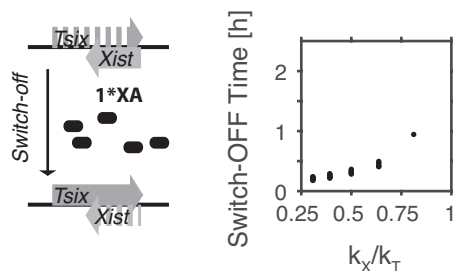### 2.3.5   Parameter rules for mono-allelic *Xist* up-regulation

In this section we analyze which parameter combinations allow monoallelic upregulation of *Xist*. As a first step we analyzed how the parameter values affected the kinetics with which the *Xist* locus switches between a repressed state and an *Xist* producing state.

Switch Times

(i) The **switch-ON time** measures how long it takes for *Xist* on a single allele to switch from a repressed state (Xa) to an *Xist* producing state (>10 RNA molecules transcribed) in the presence of a double XXA dose. For each parameter set we analyzed the average time point when one chromosome had produced 10 *Xist* molecules (=switch-ON time). If switch-on did not occur before the end of the simulation it was set to the total simulation time (100h). The switch-on time is negatively correlated with the k_X-to-k_T ratio such that a higher relative strength of *Xist* promoter compared to *Tsix* promoter results in a faster switch-ON time (Figure below).
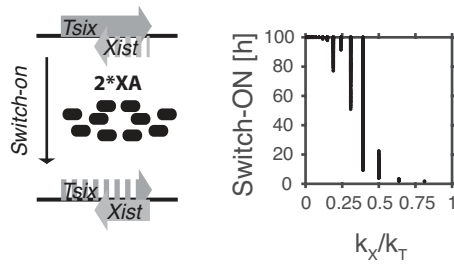
(ii) The **switch-OFF time** measures how long it takes for a single allele to switch back from an *Xist* producing state to a repressed state in the presence of a **single** XXA dose (=after XXA silencing, before *Tsix* silencing). For each parameter set 100 alleles were simulated for 500 h using the maintenance model described in section 2.2 (without *Tsix* silencing) initiating from the *Xist* producing state with the *Tsix* promoter being in the ON state. The switch-OFF time was defined as the time point when the polymerase occupancy within the *Xist* gene body is higher for *Tsix* than for *Xist*. If *Xist* switch-OFF did not occur before the end of the simulation it was set to the total simulation time. The mean switch-OFF time increases with increasing k_X-to-k_T ratios, but is always rather fast (≤1h) suggesting that *Xist* up-regulation remains unstable until *Tsix* has been silenced (Figure below).

Parameter rules

Next we defined a number of parameter rules that could identify parameter sets that could simulate mono-allelic *Xist* up-regulation. For this analysis, sets were defined as monoallelic (MA) if >90% of cells were monoallelic averaged over the last 20h of the simulation, as this can be deduced more accurately from simulating 100 individual cells than up-regulation in >99% cells. The results of this analysis are summarized in the scheme on the next page and are discussed below.

To achieve the transition from XaXa -> XaXi, a two-fold increase in k_X in the presence of a double XXA dose ($q_{XXA}=2$) must cross the activation threshold, which lies slightly below $k_X/k_T=1$ (see Fig. 2G main text). Moreover a low k_X-to-k_T ratio is associated with a slow switch-ON time (see above). The k_X-to-k_T ratio must thus be sufficiently high ($k_X/k_T ≥0.4$, group 1), otherwise *Xist* is either not swiched on or up-regulated with too slow kinetics (group 2). Within group 1 we distinguish between those sets that up-regulate *Xist* mono- (1.1) or bi-allelically (1.2), which depends on the relative kinetics of *Xist* up-regulation (swich-ON ~ k_T/k_X, see above) and XXA silencing (sil$_{XXA}$).
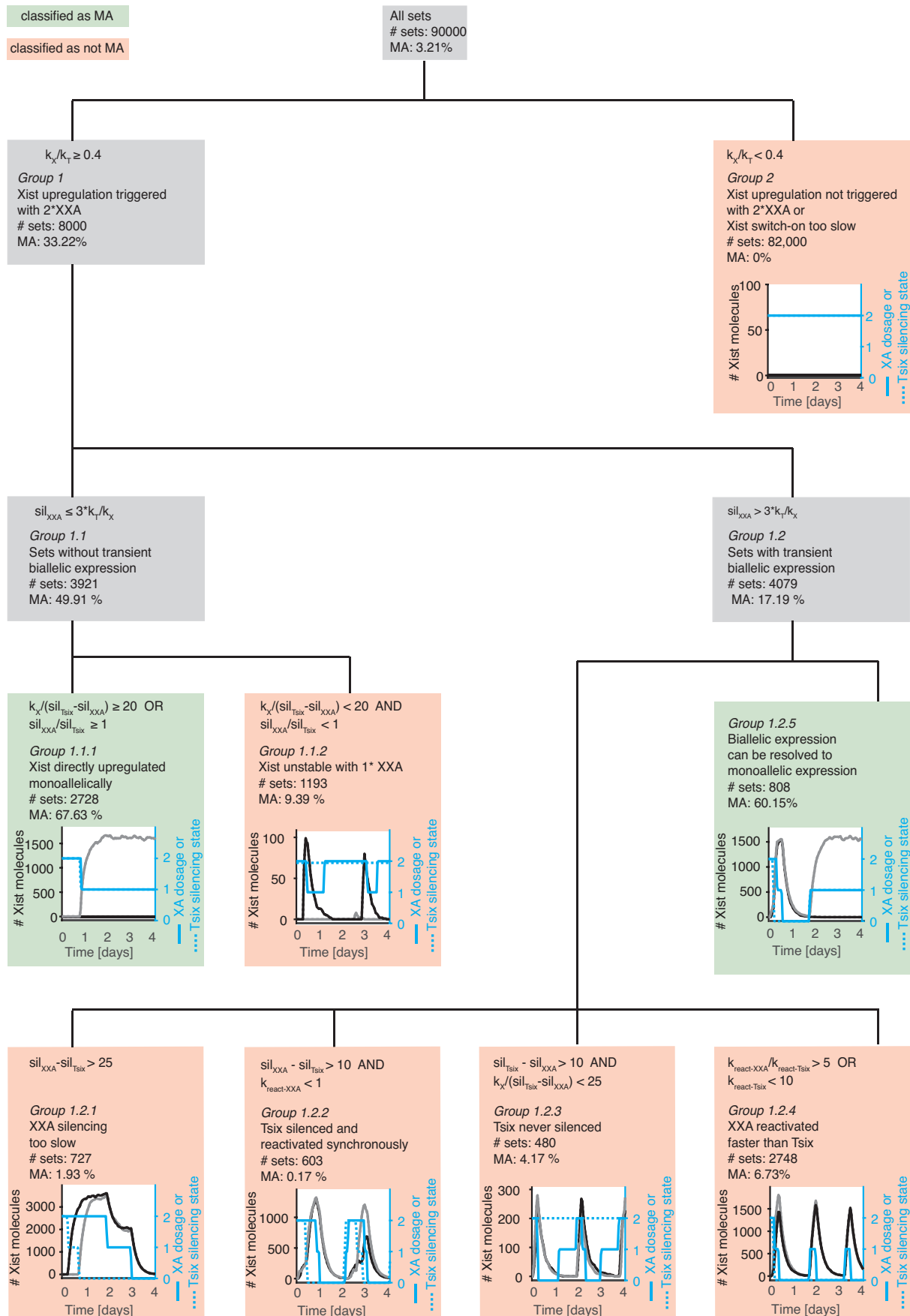
In group 1.1 *Xist* up-regulation is generally achieved except in a subgroup of sets (1.1.2) where XXA is silenced before *Tsix* (sil_{XXA}/sil_{Tsix} <1). Here *Xist* transcription is rapidly switched off in the presence of a single XXA dose (see above), if *Tsix* fails to be silenced in the time window before *Xist* RNA is cleared from the chromosome (=clearance time), which depends on the amount of *Xist* RNA present (which correlates with k_X) and the effective silencing delay (sil_{Tsix}-sil_{XXA}).

In group 1.2 *Xist* is initially up-regulated from both alleles and symmetry-breaking can thus not occur during *Xist* up-regulation. Under certain conditions however, symmetry breaking can still occur through mono-allelic silencing or reactivation of *Tsix* (1.2.5). In several scenarios however this is unlikely to occur (1.2.1-1.2.4):

- If *Tsix* is silenced much faster than XXA, both chromosomes will silence *Tsix* and symmetry-breaking cannot occur at the level of silencing (groups. 1.2.1 and 1.2.2). Symmetry breaking can still occur at the level of reactivation, except if either silencing (group 1.2.1) or reactivation (group 1.2.2) of XXA is very slow. If XXA silencing is to slow (sil_{XXA}-sil_{Tsix}>25h), *Xist* RNA can accumulate for a long time before bi-allelic XXA silencing triggers *Xist* down-regulation, such a second round of up-regulation cannot occur within the timescales that are relevant for XCI (group 1.2.1). If XXA reactivation is too slow ($k_{react-XXA}$<1h^{-1}), *Tsix* is reactivated on both alleles (1.2.2).

- If *Tsix* is silenced much more slowly than XXA (sil_{Tsix}-sil_{XXA}) and the clearance time of *Xist* is shorter than the effective silencing delay ($k_X/(sil_{Tsix}$-$sil_{XXA})$<25), both copies of XXA would be silenced resulting in *Xist* down-regulation before *Tsix* can be silenced (group 1.2.3).

- If XXA is reactivated before *Tsix* ($k_{react-XXA}/k_{react-Tsix}$>5), *Xist* is immediately upregulated from both alleles as repression in cis by *Tsix* is absent and symmetry breaking cannot occur during reactivation (1.2.4). Similarly, the order of reactivation tends to be variable for low reactivation rates ($k_{react-Tsix}$) and it cannot be ensured that *Tsix* is reactivated before XXA (1.2.4).

classified as MA

classified as not MA

All sets
sets: 90000
MA: 3.21%

$k_X/k_T \geq 0.4$
Group 1
Xist upregulation triggered with 2*XXA
sets: 8000
MA: 33.22%

$k_X/k_T < 0.4$
Group 2
Xist upregulation not triggered with 2*XXA or
Xist switch-on too slow
sets: 82,000
MA: 0%

$sil_{XXA} \leq 3*k_T/k_X$
Group 1.1
Sets without transient biallelic expression
sets: 3921
MA: 49.91 %

$sil_{XXA} > 3*k_T/k_X$
Group 1.2
Sets with transient biallelic expression
sets: 4079
MA: 17.19 %

$k_X/(sil_{Tsix}-sil_{XXA}) \geq 20$ OR $sil_{XXA}/sil_{Tsix} \geq 1$
Group 1.1.1
Xist directly upregulated monoallelically
sets: 2728
MA: 67.63 %

$k_X/(sil_{Tsix}-sil_{XXA}) < 20$ AND $sil_{XXA}/sil_{Tsix} < 1$
Group 1.1.2
Xist unstable with 1* XXA
sets: 1193
MA: 9.39 %

Group 1.2.5
Biallelic expression can be resolved to monoallelic expression
sets: 808
MA: 60.15%

$sil_{XXA}-sil_{Tsix} > 25$
Group 1.2.1
XXA silencing too slow
sets: 727
MA: 1.93 %

$sil_{XXA} - sil_{Tsix} > 10$ AND $k_{react-XXA} < 1$
Group 1.2.2
Tsix silenced and reactivated synchronously
sets: 603
MA: 0.17 %

$sil_{Tsix} - sil_{XXA} > 10$ AND $k_X/(sil_{Tsix}-sil_{XXA}) < 25$
Group 1.2.3
Tsix never silenced
sets: 480
MA: 4.17 %

$k_{react-XXA}/k_{react-Tsix} > 5$ OR $k_{react-Tsix} < 10$
Group 1.2.4
XXA reactivated faster than Tsix
sets: 2748
MA: 6.73%

By applying the rules we could correctly identify 99% of all non-monoallelic sets, while 19% of the monoallelic sets were falsely identified as non-monoallelic. The sets that were predicted monoallelic (group 1.1.1, 1.2.5) result in monoallelic expression in on average 88% of cells, and 66% of these sets were indeed monoallelic in >90% of cells. The figure below shows the distribution of monoallelic expression in all simulated sets versus the distribution in the sets predicted monoallelic by the rules.
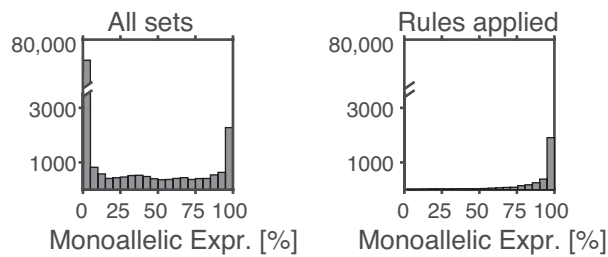
In summary, monoallelic XCI requires a tightly controlled k_X-to-k_T ratio and a symmetry breaking event between the two X chromosomes of a female cell. The silencing kinetics play a crucial role in determining whether and at which stage of XCI the break of symmetry occurs. It can either occur directly if *Xist* is monoallelically and stably upregulated from exactly one X chromosome and silences the XXA and *Tsix* in cis (slow on-switch & fast silencing) or it can occur indirectly if a transient biallelic expression state is resolved into monoallelic *Xist* expression (fast on-switch and slower silencing). This is prevented if silencing of *Tsix* and XXA occur on very different timescales.

2.4   Simulations of different genotypes

2.4.1   Identification of parameter sets compatible with experimental data

To simulate experimental data we selected a subset of parameter sets from the simulation in 2.3 that robustly led to monoallelic *Xist* upregulation (>99% cells) and were in agreement with experimental observations according to the following constraints:
 (i) The maximal percentage of bi-allelically expressing cells over the simulated time course should be below 20%
(ii) The mean *Xist* expression level must lie between 200 and 600 RNA molecules (Sun et al., 2006).
(iii) All cells up-regulate *Xist* within 48h after induction of differentiation.

Since only 34 parameter sets with unique k_X, k_T, sil_{XXA} and sil_{Tsix} combinations fulfilled these criteria, we performed another simulation to identify more parameter sets that could potentially simulate experimental data. To this end, the simulation in 2.3.4 was

repeated with additional, randomly sampled values for k_X and k_T. The parameter ranges for k_X were set such that the steady state expression level of *Xist* ($k_X/k_{X\text{-deg}}$) was between 200 and 600 molecules. Since the simulation in 2.3 revealed that monoallelic *Xist* up-regulation requires a k_X-to-k_T ratio between 0.4 and 0.8 (Fig. 3F, main text), k_T was sampled within this range. A total of 500,000 parameter sets were simulated. All parameters were sampled randomly within the ranges given in the following table.

Description	Parameter	Parameter values
Xist initiation rate [h^{-1}]	k_X	34-104 (log distributed)
Tsix initiation rate [h^{-1}]	k_T	$k_X/0.8$-$k_X/0.4$ (lin distributed)
Silencing delay of XXA [h]	sil_{XXA}	0 – 48 (log distributed)
Silencing delay of *Tsix* [h]	sil_{Tsix}	0 – 48 (log distributed)
Reactivation rate of XXA [h^{-1}]	$k_{react\text{-}XXA}$	0.1-100 (log distributed)
Reactivation rate of *Tsix* [h^{-1}]	$k_{react\text{-}T}$	0.1-100 (log distributed)

From these simulations 100 sets fulfilling the above requirements were randomly selected and were used in the following simulations.

2.4.2 Simulation of mutant cells

Xist and *Tsix* mutations were simulated as described in section 2.3 with the following modifications.

(i) *Tsix+/-*: *Tsix* initiation rate $k_T=0$ on one allele

(ii) *Tsix-/-*: *Tsix* initiation rate $k_T=0$ on both alleles.

(iii) *Xist+/-*: *Xist* initiation rate $k_X=0$ on one allele

To estimate the halftime of *Xist* up-regulation $T_{1/2}$ shown in Fig. 7E (main text) we determined the earliest time point where 50% of simulated cells had up-regulated *Xist* (>10 molecules).

2.4.3 Simulation of aneuploid cells

To simulate cells that are mono-, tri- or tetrasomic for the X-chromosome (Fig. 7H, main text), simulations were performed essentially as described in section 2.3 except that each cell contained one, three or four X-chromosomes, each contributing a single XXA-dose.

To simulate tetraploid cells (4n4X, Fig. 7J main text) we assumed that their increased nuclear size would result in an effective dilution of XXA compared to diploid cells. Each of the four X-chromosomes in a cell therefore produces only 0.5x XXA. Since only a subset of the simulated parameter sets identified in section 2.4.1 could reproduce bi-allelic *Xist* up-regulation, we attempted to better understand under which conditions the

model could predict the behavior of tetraploid cells correctly. To achieve robust inactivation of two X chromosomes, the state with only one inactive X chromosome must be unstable, meaning that the system must reside in the regime where the Xa is unstable. By contrast, with two inactive X chromosomes the cell must lie in the regime where both, Xi and Xa are stable. Thus, the requirements for robust inactivation of two X chromosomes in a 4n4X cell are more strict than for inactivation of single X in a female diploid cell as it is necessary to distinguish not only between a single and a double dosage of the XXA (100% increase) but between a double and triple dosage (50% increase) (Fig 7I, main text). To identify parameter sets that meet these criteria, we performed a maintenance simulation as described in section 2.2 for all mutant parameter sets (500h, 100 cells per set) with an XXA dosage of 0.5, 1, 1.5 and 2 to determine which of the sets were bistable with 1x XXA and monostable with a 1.5x XXA concentration. 44 out of the 100 sets fulfilled these criteria in more than 90% of cells (Fig 7I+K, blue sets). In the simulation of tetraploid cells, this group of parameter sets indeed resulted in biallelic *Xist* expression in 87% of cells on average (min 64%, max 98%) while the other sets on average led to inactivation of two X chromosomes in 56% of cells (Fig 7K). It should be noted that silencing of the XXA must be sufficiently fast to prevent inactivation of three X chromosomes. The state with XaXiXiXi is also stable as the bistable region does not possess a lower limit point.

3   References

Chaumeil, J., Augui, S., Chow, J.C., and Heard, E. (2008). Combined immunofluorescence, RNA fluorescent in situ hybridization, and DNA fluorescent in situ hybridization to study chromatin changes, transcriptional activity, nuclear organization, and X-chromosome inactivation. Methods Mol. Biol. *463*, 297–308.

Chow, J.C., Ciaudo, C., Fazzari, M.J., Mise, N., Servant, N., Glass, J.L., Attreed, M., Avner, P., Wutz, A., Barillot, E., et al. (2010). LINE-1 activity in facultative heterochromatin formation during X chromosome inactivation. Cell *141*, 956–969.

Gillespie, D.T. (1977). Exact stochastic simulation of coupled chemical reactions. The Journal of Physical Chemistry *81*, 2340–2361.

Giorgetti, L., Galupa, R., Nora, E.P., Piolot, T., Lam, F., Dekker, J., Tiana, G., and Heard, E. (2014). Predictive polymer modeling reveals coupled fluctuations in chromosome conformation and transcription. Cell *157*, 950–963.

Jonkers, I., Kwak, H., Lis, J.T., and Struhl, K. (2014). Genome-wide dynamics of Pol II elongation and its interplay with promoter proximal pausing, chromatin, and exons. Elife *3*, e02407.

Okamoto, I., Otte, A.P., Allis, C.D., Reinberg, D., and Heard, E. (2004). Epigenetic dynamics of imprinted X inactivation during early mouse development. Science *303*, 644–649.

Ran, F.A., Hsu, P.D., Wright, J., Agarwala, V., Scott, D.A., and Zhang, F. (2013). Genome engineering using the CRISPR-Cas9 system. Nat Protoc *8*, 2281–2308.

Schulz, E.G., Meisig, J., Nakamura, T., Okamoto, I., Sieber, A., Picard, C., Borensztein, M., Saitou, M., Blüthgen, N., and Heard, E. (2014). The Two Active X Chromosomes in Female ESCs Block Exit from the Pluripotent State by Modulating the ESC Signaling Network. Cell Stem Cell *14*, 203–216.

Sun, B.K., Deaton, A.M., and Lee, J.T. (2006). A Transient Heterochromatic State in Xist Preempts X Inactivation Choice without RNA Stabilization. Molecular Cell *21*, 617–628.

Wutz, A., Rasmussen, T.P., and Jaenisch, R. (2002). Chromosomal silencing and localization are mediated by different domains of Xist RNA. Nature Genetics *30*, 167–174.

Yamada, N., Hasegawa, Y., Yue, M., Hamada, T., Nakagawa, S., and Ogawa, Y. (2015). Xist Exon 7 Contributes to the Stable Localization of Xist RNA on the Inactive X-Chromosome. PLoS Genet. *11*, e1005430.